

# Exact and general decoupled solutions of the LMC Multitask Gaussian Process model

Olivier Truffinet<sup>1</sup>, Karim Ammar<sup>1</sup>, Jean-Philippe Argaud<sup>2</sup>, and Bertrand Bouriquet<sup>3</sup>

<sup>1</sup>Université Paris-Saclay, CEA, Service d'Études des Réacteurs et de Mathématiques Appliquées, 91190, Gif-sur-Yvette, France

<sup>2</sup>EDF R& D, 91120, Palaiseau, France,

<sup>3</sup>EDF,

March 22, 2024

## Abstract

The Linear Model of Co-regionalization (LMC) is a very general model of multitask gaussian process for regression or classification. While its expressivity and conceptual simplicity are appealing, naive implementations have cubic complexity in the number of datapoints and number of tasks, making approximations mandatory for most applications. However, recent work has shown that under some conditions the latent processes of the model can be decoupled, leading to a complexity that is only linear in the number of said processes. We here extend these results, showing from the most general assumptions that the only condition necessary to an efficient exact computation of the LMC is a mild hypothesis on the noise model. We introduce a full parametrization of the resulting *projected LMC* model, and an expression of the marginal likelihood enabling efficient optimization. We test this new model on real and synthetic data, performing a parametric study on the latter to assess the severity of the noise model restriction. Overall, the projected LMC appears as a viable and simpler alternative to state-of-the art models, which greatly facilitates some computations such as leave-one-out cross-validation and fantasization.

## 1 Introduction

Multi-Outputs Gaussian Processes (MOGP) are popular tools for learning linearly correlated quantities. They find use in many fields : earth and climate sciences, robotics, surrogate modeling... Some recent successful applications include modeling of electrical motors (Wen et al. [2021]), indoor localization (Tang et al. [2022]), solar power prediction (Dahl and Bonilla [2019]), and inverse problem resolution for a centrifugal pump blade (Zhang and Zhao [2020]). They even provide full paradigms for tasks such as uncertainty quantification (Bilionis et al. [2013]) and Bayesian optimization (Maddox et al. [2021]). As described in a recent survey of MOGPs (Liu et al. [2018]), the vast majority of models operating in the most straightforward setup – supervised learning of several tasks, all akin to each other and treated in the same fashion – fall into two main categories: this of *convolutional GPs* and this of *linearly correlated GPs*. The latter can essentially be grouped under the term "*Linear model of co-regionalization*" (LMC).

The LMC stems from a very natural idea, this of modelizing all observed outputs as linear combinations of common unobserved and independant gaussian processes. From an equivalent perspective,

the outputs can also be viewed as a vector-valued function, which follows a multidimensional gaussian process with vectorial mean and matricial kernel function (Alvarez et al. [2012]); then the equations of single-output GPs apply to this model, modulo a flattening of some matricial quantities. However, **this procedure scales as  $\mathcal{O}((np)^3)$**  both for training and inference, making it intractable in most cases. Several methods have therefore been developed to circumvent this limitation, which rely on two complementary approaches: either **restricting the model to some particular case that is more amenable to computation**, reducing its expressivity, or **approximating some of its parts**, thus degrading its accuracy. The first category includes the *intrinsic coregionalization model* (ICM), sometimes referred to as Multi-Task Gaussian Process (Bonilla et al. [2007]), where all latent processes are restricted to have the same kernel, and both the Orthogonal Instantaneous Linear Mixing Model (OILMM, Bruinsma et al. [2020]) and the Generalized Probabilistic Principal Component Analysis (GPPCA, Gu and Shen [2020]), in which the mixing matrix encoding correlations between outputs is constrained to be orthogonal. Models of the second category often resort to *variational approaches* (Bonilla et al. [2019]), which introduce an approximate form for the posterior of latent processes and optimize a lower bound of the marginal log-likelihood instead of this quantity itself; they include the pioneer Semiparametric Latent Factor Model (Teh et al. [2005]) and the Collaborative multi-output Gaussian Process (Houlsby et al. [2012]). We emphasize that all of the cited methods are *subcases or approximations* of the LMC, not distinct models that would extend its generality. Let’s finally mention that massive work has also been undertaken to improve the scalability of single-output GPs (see for instance the review of Liu et al. [2020]), which also benefits to multi-output ones – variational approximation for instance have first been introduced for the single-output case.

The present work generalizes two recent publications introducing respectively the OILMM and the GPPCA (see above paragraph). As their authors

point it out, these models are subcases of the LMC where assumptions are made on the noise model, and more importantly on the mixing matrix, which is constrained to have orthogonal or orthonormal columns. However, it happens that **this assumption of orthogonality is unnecessary**: exact and convenient computation of the model can be carried without it, at the expense of a slightly more complex treatment of the noise. This is the main finding motivating the present article.

The main contributions of this paper are as follows:

- We write general expressions for LMC posteriors at the level of latent processes, and show how they can be efficiently computed if a specific condition on the noise model is enforced;
- We find a general form for noise matrices enforcing this condition, compute and optimize the marginal log-likelihood of the model given this parametrization;
- We demonstrate the validity of our approach by comparing the resulting projected LMC to concurrent simplifications; in particular, we undertake a parametric study on synthetic data to assess the effects of the noise hypothesis in various setups.

## 2 Background and notations

A generic LMC model is specified by  $\mathbf{y} = \mathbf{H}\mathbf{u} + \boldsymbol{\epsilon}$ , with  $\mathbf{H}$  a  $p \times q$  mixing matrix without any specific property,  $\mathbf{u} = (u_1, \dots, u_q)^T \in \mathbb{R}^q$  such that  $u_i \sim \mathcal{GP}(0, k_i)$  and priors of the  $u_i$ ’s are mutually independent, and  $\boldsymbol{\epsilon} \sim \mathcal{N}(0, \boldsymbol{\Sigma})$  with  $\boldsymbol{\Sigma} \in \mathbb{R}^{p \times p}$  an inter-task noise matrix which is symmetric but not necessarily diagonal. We also note  $\mathbf{X} \in \mathbb{R}^{d \times n}$  the matrix of  $d$ -dimensional input points,  $\mathbf{Y} \in \mathbb{R}^{p \times n}$  this of the  $p$  data outputs,  $\mathbf{U} \in \mathbb{R}^{q \times n}$  the values of the  $q$  latent processes at observation points,  $\text{vec}(\mathbf{M})$  the vectorization of the matrix  $\mathbf{M}$  (i.e its column-wise unfolding),  $\mathbf{M}_{\mathbf{v}} = \text{vec}(\mathbf{M}^T)$ ,  $\mathbf{x}_*$  a test point for prediction,  $\Phi$  the probabilistic estimator of random variable  $\Phi$ ,  $\mathbf{k}_{i*} = (k_i(\mathbf{x}_*, \mathbf{x}_j))_{1 \leq j \leq n}$  and  $k_{i**} = k_i(\mathbf{x}_*, \mathbf{x}_*)$  the

train/test covariance vector and test-test variance for kernel  $i$ ,  $\text{Diag}(\mathbf{K}_i)$  the block-diagonal matrix where the  $i$ -th block is the kernel matrix  $\mathbf{K}_i$  (the subscript indicating iteration on  $i$  is omitted), and  $\otimes$  the Kronecker product. For simplicity, **we restrict ourselves to the case of zero-mean GPs**: the case of a general sum-of-regressors mean function, significantly more convoluted and useful only in peculiar setups, will be the matter of future work.

The naive exact implementation of the LMC is then written (Alvarez et al. [2012]):

$$p(\mathbf{y}_*|\mathbf{Y}) = \mathcal{N}(\mathbf{k}_*^T \mathcal{K}^{-1} \mathbf{Y}_v, \mathbf{k}_{**} - \mathbf{k}_*^T \mathcal{K}^{-1} \mathbf{k}_*) \quad (1)$$

$$-2 \log p(\mathbf{Y}) = \mathbf{Y}_v^T \mathcal{K}^{-1} \mathbf{Y}_v + \log |\mathcal{K}| + \frac{np}{2} \log \pi \quad (2)$$

for respectively predictions at a new point  $\mathbf{y}_*$  and the marginal log-likelihood, with  $\mathcal{K} = (\mathbf{H} \otimes \mathbf{I}_n) \text{Diag}(\mathbf{K}_i) (\mathbf{H}^T \otimes \mathbf{I}_n) + \Sigma \otimes \mathbf{I}_n$  the noise-added cross-tasks covariance matrix. This is formally equivalent to the computation of a single-output GP, but with the burden of handling an  $(np \times np)$  matrix in all operations.

### 3 Latent-revealing expressions of LMC estimators

We now present new exact expressions for the LMC which highlight its low-rank structure. These are derived in all generality.

#### 3.1 Posteriors

**Proposition 1.** *The posterior  $p(\mathbf{U}_v|\mathbf{Y})$  of the latent processes  $\mathbf{U}$  at the training points is gaussian with mean and variance:*

$$\mathbb{E}(\mathbf{U}_v|\mathbf{Y}) = [\text{Diag}(\mathbf{K}_i^{-1}) + \mathbf{H}^T \Sigma^{-1} \mathbf{H} \otimes \mathbf{I}_n]^{-1} \cdot \text{vec}(\mathbf{Y}^T \Sigma^{-1} \mathbf{H})$$

$$\mathbb{V}(\mathbf{U}_v|\mathbf{Y}) = (\text{Diag}(\mathbf{K}_i^{-1}) + \mathbf{H}^T \Sigma^{-1} \mathbf{H} \otimes \mathbf{I}_n)^{-1} \quad (3)$$

**Remark 1.** *It can be noted that 3 is only a block-wise version of the result (2.116) of Bishop's textbook*

(Bishop [2006]) for the conditional law of a linear combination of joint gaussian variables, applied here with  $\mathbf{x} = \mathbf{U}_v$ ,  $\mathbf{A} = \mathbf{H}$ ,  $\mathbf{L} = \Sigma^{-1}$ ,  $\mathbf{\Lambda} = \text{Diag}(\mathbf{K}_i^{-1})$  and  $\boldsymbol{\mu} = \mathbf{0}$ ,  $\mathbf{b} = \mathbf{0}$ . The only difference is that the vectors  $\mathbf{x}$  and  $\mathbf{y}$  in this result contain one value per "task", whereas our vectors  $\mathbf{U}_v$  and  $\mathbf{Y}_v$  contain gaussian subvectors of size  $n$ .

Let  $\hat{\mathbf{y}}_*$  be our estimator for  $\mathbf{Y}$  at test point  $\mathbf{x}_*$  and  $\hat{\mathbf{u}}_*$  this for  $\mathbf{U}$ . As  $\mathbf{H}$  is considered deterministic, we have  $p(\hat{\mathbf{y}}_*|\mathbf{Y}) = p(\mathbf{H}\hat{\mathbf{u}}_*|\mathbf{Y}) = \mathcal{N}(\mathbf{H}\mathbb{E}(\hat{\mathbf{u}}_*|\mathbf{Y}), \mathbf{H}\mathbb{V}(\hat{\mathbf{u}}_*|\mathbf{Y})\mathbf{H}^T)$ . Therefore, the only quantity still required for prediction is  $p(\hat{\mathbf{u}}_*|\mathbf{Y})$ . This is done in the following proposition:

**Proposition 2.**  *$p(\hat{\mathbf{u}}_*|\mathbf{Y})$  is gaussian with respective mean and variance:*

$$\mathbb{E}(\hat{\mathbf{u}}_*|\mathbf{Y}) = \mathfrak{K} [\mathbb{K} + (\mathbf{H}^T \Sigma^{-1} \mathbf{H})^{-1} \otimes \mathbf{I}_n]^{-1} \cdot \text{vec}(\mathbf{Y}^T \Sigma^{-1} \mathbf{H} (\mathbf{H}^T \Sigma^{-1} \mathbf{H})^{-1})$$

$$\mathbb{V}(\hat{\mathbf{u}}_*|\mathbf{Y}) = \mathbf{k}_d - \mathfrak{K} [\mathbb{K} + (\mathbf{H}^T \Sigma^{-1} \mathbf{H})^{-1} \otimes \mathbf{I}_n]^{-1} \mathfrak{K} \quad (4)$$

with further notations  $\mathbb{K} = \text{Diag}(\mathbf{K}_i)$ ,  $\mathfrak{K} = \text{Diag}(\mathbf{k}_{i*})$  and  $\mathbf{k}_d = \text{Diag}(k_{i**})$  for compacity.

These expressions are very close to a block-diagonal version of a single-output GP. Two quantities stand out from them: a term  $(\mathbf{H}^T \Sigma^{-1} \mathbf{H})^{-1}$  which seems to play the role of a noise for the latent processes, and a matrix  $(\mathbf{H}^T \Sigma^{-1} \mathbf{H})^{-1} \mathbf{H}^T \Sigma^{-1} \mathbf{Y}$  which appears to act as a  $q$ -dimensional summary of the data. We therefore set the following notations:

**Definition 1.** *We note  $\Sigma_{\mathbf{P}} = (\mathbf{H}^T \Sigma^{-1} \mathbf{H})^{-1}$  and  $\mathbf{T} = (\mathbf{H}^T \Sigma^{-1} \mathbf{H})^{-1} \mathbf{H}^T \Sigma^{-1} = \Sigma_{\mathbf{P}} \mathbf{H}^T \Sigma^{-1}$ .*

#### 3.2 Likelihood

In the same vein as the above expressions, the following formula from Bruinsma expresses the likelihood at the level of the latent processes rather than the observable tasks. Remarkably,  $\Sigma_{\mathbf{P}}$  and  $\mathbf{T}\mathbf{Y}$  are also key here.

**Proposition 3.** *The likelihood of the data can be decomposed as the likelihood of the projected data multiplied by a corrective term accounting for projection*

loss, independent of the latent processes:

$$p(\mathbf{Y}) = \prod_{j=1}^n \frac{\mathcal{N}(\mathbf{Y}_j | \mathbf{0}, \boldsymbol{\Sigma})}{\mathcal{N}(\mathbf{T}\mathbf{Y}_j | \mathbf{0}, \boldsymbol{\Sigma}_{\mathbf{P}})} \times \int p(\mathbf{U}) \prod_{j=1}^n \mathcal{N}(\mathbf{T}\mathbf{Y}_j | \mathbf{U}_j, \boldsymbol{\Sigma}_{\mathbf{P}}) d\mathbf{U} \quad (5)$$

(where  $\mathbf{Y}_j$ ,  $\mathbf{U}_j$  denote the rows of  $\mathbf{Y}$  and  $\mathbf{U}$  respectively, associated with datapoint  $j$ ).

The derivation of (5) in Bruinsma et al. [2020] is quite clever and requires prior investigation of  $\boldsymbol{\Sigma}_{\mathbf{P}}$  and  $\mathbf{T}\mathbf{Y}$ . However, a similar expression can be derived from elementary considerations and is displayed in Annex F.

### 3.3 Decoupled expressions

We have derived so far exact expressions for all quantities of the model, expressed at the level of latent processes; but these expressions are not necessarily cheaper to compute than their "naive" counterpart (1). Looking at  $\mathbb{E}(\hat{\mathbf{u}}_* | \mathbf{Y})$  and  $\mathbb{V}(\hat{\mathbf{u}}_* | \mathbf{Y})$ , it appears that they consist in products of block-diagonal matrices and a single large  $nq \times nq$  matrix,  $\mathcal{K}^{-1} = [\mathbf{Diag}(\mathbf{K}_i) + \boldsymbol{\Sigma}_{\mathbf{P}} \otimes \mathbf{I}_n]^{-1}$ . By writing  $p(\hat{\mathbf{y}}_* | \mathbf{Y})$  as  $\mathcal{N}(\mathbf{H}\mathbb{E}(\hat{\mathbf{u}}_* | \mathbf{Y}), \mathbf{H}\mathbb{V}(\hat{\mathbf{u}}_* | \mathbf{Y})\mathbf{H}^T)$ , we have thus reduced time complexity from  $O(n^3p^3)$  to  $O(n^3q^3)$ , but there is a much more crucial observation: **a necessary and sufficient condition for  $\mathcal{K}$  to be block-diagonal is that  $\boldsymbol{\Sigma}_{\mathbf{P}}$  be diagonal**. We frame this condition as of now given its importance in the rest of the article:

**Definition 2.** We say that  $\boldsymbol{\Sigma}$  is a diagonally projectable noise for  $\mathbf{H}$ , abbreviated as DPN, if  $\mathbf{H}^T\boldsymbol{\Sigma}^{-1}\mathbf{H}$  is diagonal.

It follows immediately that if the DPN assumption is verified, the estimators of prop. 2 decouple, that is, we can express the component  $p(\hat{u}_{i*} | \mathbf{Y})$  in function of only  $k_i$  and a specific projection of  $\mathbf{Y}$  of size  $n$ :

**Proposition 4.** If the DPN condition stands, we have the following decoupled expression for the poste-

rior of each latent process:

$$p(\hat{u}_{i*} | \mathbf{Y}) = \mathcal{N}(k_{i**} - \mathbf{k}_{i*}^T(\mathbf{K}_i + \sigma_i^2\mathbf{I}_n)^{-1}\mathbf{T}_i\mathbf{Y}, k_{i**} - \mathbf{k}_{i*}^T(\mathbf{K}_i + \sigma_i^2\mathbf{I}_n)^{-1}\mathbf{k}_{i*}) \quad (6)$$

with  $\boldsymbol{\Sigma}_{\mathbf{P}} = (\mathbf{H}^T\boldsymbol{\Sigma}^{-1}\mathbf{H})^{-1} = \text{Diag}(\sigma_i^2)_{1 \leq i \leq q}$  and  $\mathbf{T}_i$  the  $i$ -th row of  $\mathbf{T}$ .

This is the expression of a standard single-out GP posterior and can thus be computed with time complexity  $O(n^3)$  per latent process.

It can also be seen easily from equation (5) that the likelihood factorizes over latent processes if and only if  $\mathcal{N}(\mathbf{T}\mathbf{Y}_j | \mathbf{U}_j, \boldsymbol{\Sigma}_{\mathbf{P}})$  does, i.e if  $\boldsymbol{\Sigma}_{\mathbf{P}}$  is diagonal. In this case  $\mathcal{N}(\mathbf{T}\mathbf{Y}_j | \mathbf{U}_j, \boldsymbol{\Sigma}_{\mathbf{P}}) = \prod_{i=1}^q \mathcal{N}(\mathbf{T}_i^T\mathbf{Y}_j | U_{ij}, \sigma_i^2)$ , which is again a standard GP term.

**Remark 2.** As latent processes have regular single-output GP expressions under the DPN hypothesis, any GP approximation (typically inducing points) can be "plugged" onto the estimators of prop.4 in order to further reduce computational complexity.

### 3.4 Probabilistic interpretation

The recurrence of quantities  $\boldsymbol{\Sigma}_{\mathbf{P}}$  and  $\mathbf{T}\mathbf{Y}$  in all previous expressions<sup>1</sup> hints that they have a probabilistic meaning. The next proposition gives such an interpretation, mostly restating results from Bruinsma et al. [2020].

**Proposition 5.** •  $\mathbf{T}$  is a generalized inverse of  $\mathbf{H}$ :  $\mathbf{T}\mathbf{H} = \mathbf{I}_q$ . Therefore,  $\mathbf{H}\mathbf{T}$  is a projection.

- $\mathbf{T}\mathbf{Y}$  is a maximum likelihood estimator for  $\mathbf{U}$ :  $\mathbf{T}\mathbf{Y} = \arg \max_{\mathbf{U}} p(\mathbf{Y} | \mathbf{U})$ . It is an unbiased estimator:  $\mathbb{E}[\mathbf{T}\mathbf{Y} | \mathbf{U}] = \mathbf{U}$ .
- $\mathbf{T}\mathbf{Y}$  is a minimal sufficient statistic of the data  $\mathbf{Y}$  for the variable  $\mathbf{U}$ . In other words,  $\mathbf{T}\mathbf{Y}$  contains all the information required to compute the best possible estimate of  $\mathbf{U}$ . Consequently,  $p(\mathbf{U} | \mathbf{Y}) = p(\mathbf{U} | \mathbf{T}\mathbf{Y})$ .

<sup>1</sup>Equation (3) can be rephrased as  $\mathbb{E}(\mathbf{U}_v | \mathbf{Y}) = [\mathbf{Diag}(\mathbf{K}_i^{-1}) + \boldsymbol{\Sigma}_{\mathbf{P}}^{-1} \otimes \mathbf{I}_n]^{-1} \text{vec}(\mathbf{Y}\mathbf{T}^T\boldsymbol{\Sigma}_{\mathbf{P}}^{-1})$ ,  $\mathbb{V}(\mathbf{U}_v | \mathbf{Y}) = (\mathbf{Diag}(\mathbf{K}_i^{-1}) + \boldsymbol{\Sigma}_{\mathbf{P}}^{-1} \otimes \mathbf{I}_n)^{-1}$ .

- $\mathbf{T}\Sigma\mathbf{T}^T = \Sigma_{\mathbf{P}}$ , so that  $\mathbf{T}\mathbf{Y}|\mathbf{U} \sim \mathcal{N}(\mathbf{U}_{\mathbf{v}}, \Sigma_{\mathbf{P}} \otimes \mathbf{I}_n)$
- The latent processes of any LMC model are independent conditionally upon observations if and only if  $\Sigma_{\mathbf{P}}$  is diagonal.

## 4 The diagonally-projected noise condition

We have not given so far a procedure for optimizing the likelihood, because this requires a joint parametrization of  $\mathbf{H}$  and  $\Sigma$ : these matrices are coupled by the DPN condition, so they cannot be optimized independently. This is the matter of the present section. We emphasize that *the main goal of this analysis is not to explore complex noise structures, but to allow for a decoupled model while maintaining a fully general  $\mathbf{H}$ .* It happens that this requirement puts constraint on the noise covariance  $\Sigma$ ; for instance, **the model is no longer compatible in general with a diagonal  $\Sigma$  matrix** (independent per-task noises).

### 4.1 Characterization of diagonally-projected noises

Reminding that the DPN assumption 2 is written ( $\mathbf{H}^T \Sigma^{-1} \mathbf{H}$  is diagonal), we hint that it can be expressed as some orthogonality condition between rows of  $\Sigma^{-1}$  and columns of  $\mathbf{H}$ . We therefore introduce the QR decomposition of  $\mathbf{H}$ :  $\mathbf{H} = \mathbf{Q}\mathbf{R}$ , where  $\mathbf{Q}$  has orthonormal columns and shape  $p \times q$ , and  $\mathbf{R}$  is upper-triangular of size  $q \times q$ . We also introduce  $\mathbf{Q}_{\perp}$ , a  $p \times (p - q)$  orthonormal complement of  $\mathbf{Q}$  which for now is arbitrary. We state the following lemma:

**Lemma 1.** *Any symmetric matrix  $S$  can be decomposed as  $S = \mathbf{Q}\mathbf{A}\mathbf{Q}^T + \mathbf{Q}_{\perp}\mathbf{B}\mathbf{Q}_{\perp}^T + \mathbf{Q}\mathbf{C}\mathbf{Q}_{\perp}^T + \mathbf{Q}_{\perp}\mathbf{C}^T\mathbf{Q}^T$ , with  $\mathbf{A}, \mathbf{B}$  symmetric matrices and  $\mathbf{C}$  a  $q \times (p - q)$  matrix.*

A first characterization of the DPN condition follows:

**Proposition 6.** *Let  $\Sigma^{-1} = \mathbf{Q}\mathbf{A}\mathbf{Q}^T + \mathbf{Q}_{\perp}\mathbf{B}\mathbf{Q}_{\perp}^T + \mathbf{Q}\mathbf{C}\mathbf{Q}_{\perp}^T + \mathbf{Q}_{\perp}\mathbf{C}^T\mathbf{Q}^T$  be a decomposition of  $\Sigma^{-1}$  as in lemma 1. Then  $\Sigma_{\mathbf{P}} = \mathbf{R}^{-1}\mathbf{A}^{-1}\mathbf{R}^{-T}$ , (where  $\mathbf{R}^{-T}$  denotes the inverse transpose of  $\mathbf{R}$ ) and the DPN condition is equivalent to  $(\mathbf{A} = \mathbf{R}^{-T}\mathbf{D}\mathbf{R}^{-1})$  for some diagonal matrix  $\mathbf{D}$  of size  $q$ .*

**Remark 3.** *Notice that  $\mathbf{A}, \mathbf{B}$  and  $\mathbf{C}$  are simply sub-blocks of  $\Sigma^{-1}$  in the basis spanned by  $\mathbf{Q}$  and  $\mathbf{Q}_{\perp}$ , and that  $\mathbf{B}$  and  $\mathbf{C}$  remain arbitrary: the DPN condition only involves a  $q \times q$  submatrix of  $\Sigma^{-1}$ , with  $q \ll p$  in most cases. This observation, which hints the benign nature of this assumption, is made more precise in Annex G, where a closed-form expression of the optimal  $\mathbf{D}$  and a noise correction procedure are provided.*

Computations with the LMC involve both  $\Sigma^{-1}$  and  $\Sigma$ , therefore we seek a factorized rather than additive form for  $\Sigma^{-1}$ .

**Proposition 7.** *Given its decomposition 1, the following factorization stands for any symmetric matrix  $\Sigma^{-1}$ :*

$$\Sigma^{-1} = \mathbf{Q}_+ \mathbf{R}_+^{-T} \mathbf{D}_+^{-1} \mathbf{R}_+^{-1} \mathbf{Q}_+^T, \quad (7)$$

where:  $\mathbf{Q}_+ = (\mathbf{Q} \mid \mathbf{Q}_{\perp})$ ,  $\mathbf{R}_+ = \begin{pmatrix} \mathbf{R} & \mathbf{0} \\ \mathbf{0} & \mathbf{I}_{p-q} \end{pmatrix}$ ,

$$\mathbf{D}_+^{-1} = \begin{pmatrix} \mathbf{D} & \mathbf{M} \\ \mathbf{M}^T & \mathbf{B} \end{pmatrix}, \quad \mathbf{D} = \mathbf{R}^T \mathbf{A} \mathbf{R} \quad \text{and}$$

$\mathbf{M} = \mathbf{R}^T \mathbf{C}$ . *By construction  $\mathbf{Q}_+$  is a  $p \times p$  orthonormal matrix and  $\mathbf{R}_+$  is a  $p \times p$  upper triangular matrix. By prop.6,  $\mathbf{D} = \Sigma_{\mathbf{P}}^{-1}$ , so it is diagonal if and only if the DPN condition stands.*

**Corollary 1.**

$$\Sigma = \mathbf{Q}_+ \mathbf{R}_+ \mathbf{D}_+ \mathbf{R}_+^T \mathbf{Q}_+^T, \quad (8)$$

where the blocks of  $\mathbf{D}_+$  are denoted  $\mathbf{D}_+ = \begin{pmatrix} \tilde{\mathbf{D}} & \tilde{\mathbf{M}} \\ \tilde{\mathbf{M}}^T & \tilde{\mathbf{B}} \end{pmatrix}$  and can be computed from block-wise inversion formulas.

If we decompose  $\Sigma$  in the way of lemma 1, that is  $\Sigma = \mathbf{Q}\tilde{\mathbf{A}}\mathbf{Q}^T + \mathbf{Q}_{\perp}\tilde{\mathbf{B}}\mathbf{Q}_{\perp}^T + \mathbf{Q}\tilde{\mathbf{C}}\mathbf{Q}_{\perp}^T + \mathbf{Q}_{\perp}\tilde{\mathbf{C}}^T\mathbf{Q}^T$ , noticing the formal analogy between the above factorization and this of  $\Sigma^{-1}$  (inverting  $\mathbf{R}$  and  $\mathbf{R}^{-T}$ ), we get from prop.7 that  $\tilde{\mathbf{D}} = \mathbf{R}^{-1}\tilde{\mathbf{A}}\mathbf{R}^{-T}$  and  $\tilde{\mathbf{M}} = \mathbf{R}^{-1}\tilde{\mathbf{C}}$ .

**Proposition 8.**  $\tilde{\mathbf{B}}^{-1}$ ,  $\Sigma_{\mathbf{P}}$  and  $\mathbf{M}$  form a full parametrization of the noise matrix  $\Sigma$  and can be optimized independently. Moreover,  $\Sigma$  is enforced to be p.s.d. if and only if  $\Sigma_{\mathbf{P}}$  and  $\tilde{\mathbf{B}}$  are parametrized to be respectively positive and p.s.d.

This parametrization also yields valuable insight about the model. For instance, we have the following expressions for  $\mathbf{T}$ , which connects it to the pseudoinverse of  $\mathbf{H}$ :

**Proposition 9.**

$$\mathbf{T} = \mathbf{H}^+ + \Sigma_{\mathbf{P}} \mathbf{H}^T \mathbf{Q} \mathbf{C} \mathbf{Q}_{\perp}^T = \mathbf{R}^{-1} \mathbf{Q}^T + \Sigma_{\mathbf{P}} \mathbf{M} \mathbf{Q}_{\perp}^T \quad (9)$$

where  $\mathbf{H}^+$  is the Moore-Penrose pseudoinverse of  $\mathbf{H}$ . These expressions don't depend on a particular choice of the orthogonal complement  $\mathbf{Q}_{\perp}$ .

**Corollary 2.** If  $\mathbf{C} = \mathbf{Q}^T \Sigma \mathbf{Q}_{\perp} = \mathbf{0}$ , all expressions greatly simplify:  $\mathbf{T} = \mathbf{H}^+$ ,  $\mathbf{M} = \mathbf{0}$ ,  $\tilde{\mathbf{M}} = \mathbf{0}$ ,  $\tilde{\mathbf{D}} = \mathbf{D}^{-1}$ ,  $\tilde{\mathbf{B}} = \mathbf{B}^{-1}$ . We name this case the **block-diagonal noise assumption (BDN)**; it is equivalent to setting  $\mathbf{M} = \mathbf{0}$ .

## 4.2 Optimization of the marginal log-likelihood

**Proposition 10.** Under the DPN condition, we have the following decoupled expression for the marginal log-likelihood (which doesn't depend on a particular choice of the orthogonal complement  $\mathbf{Q}_{\perp}$ ):

$$\begin{aligned} -2 \log p(\mathbf{Y}) &= (p-q)n \log 2\pi + 2n \log |\mathbf{R}| + n \log |\tilde{\mathbf{B}}| \\ &+ \text{Tr}(\mathbf{Y}^T \mathbf{Q}_{\perp} \tilde{\mathbf{B}}^{-1} \mathbf{Q}_{\perp}^T \mathbf{Y}) + \sum_{i=1}^q \log \mathcal{N}(\mathbf{T}_i \mathbf{Y} | \mathbf{0}, \mathbf{K}_i + \sigma_i \mathbf{I}_n) \end{aligned} \quad (10)$$

**Remark 4.** Notice that  $\mathbf{M}$  and  $\tilde{\mathbf{B}}$  are noise parameters, which are likely to be of low magnitude and low relevance to the model:  $\tilde{\mathbf{B}}$  can be seen as a "discarded noise" which is absent from the posteriors and acts on the likelihood essentially by interfering with  $\mathbf{Q}_{\perp}$ , while  $\mathbf{M}$  couples the projected noise with the discarded noise. We can therefore try to further simplify the model, for instance by setting  $\mathbf{M} = \mathbf{0}$  (BDN assumption, see corollary 2) or assuming  $\tilde{\mathbf{B}}$  to be scalar or

diagonal. In fact, the latter assumption is not even restrictive, as the following proposition shows:

**Proposition 11.** The projection matrix  $\mathbf{T}$  and posteriors of the model don't depend on  $\tilde{\mathbf{B}}$ ; moreover,  $\tilde{\mathbf{B}}$  can be restricted to be diagonal without incidence on the likelihood.

Even if the suggested simplifications had little impact on the values of estimators, they could modify the behavior of parameter optimization. One objective of the upcoming experimental section will be to assess which of them should be favored in practice.

Noting from prop.(9) that  $\mathbf{T} = \mathbf{R}^{-1} \mathbf{Q}^T + \Sigma_{\mathbf{P}} \mathbf{M} \mathbf{Q}_{\perp}^T$ , and setting  $\tilde{\mathbf{B}}^{-1} = \mathbf{L} \mathbf{L}^T$  to be the Cholesky decomposition of  $\tilde{\mathbf{B}}^{-1}$ , we can finally select the following parameters for the model, which we from now on refer to as **projected LMC** or **PLMC**:

- An orthonormal  $p \times p$  matrix  $\mathbf{Q}_+$  (joint optimization of  $\mathbf{Q}$  and  $\mathbf{Q}_{\perp}$ )<sup>2</sup>;
- An upper-triangular, positive-diagonal  $q \times q$  matrix  $\mathbf{R}$ ;
- A  $(p-q) \times (p-q)$  Cholesky factor  $\mathbf{L}$  which by prop.11 can be assumed diagonal, optimization considerations aside;
- A  $q \times (p-q)$  matrix  $\mathbf{M}$  with no specific property;
- A  $q \times q$  positive diagonal matrix  $\Sigma_{\mathbf{P}}$ , integrated to the parameters of the latent GPs ( $\sigma_i$ 's of prop. 4);
- All parameters of the latent kernels  $\mathbf{K}_i$ .

**Remark 5.** In Bruinsma et al. [2020], the mixing matrix of the OILMM is written  $\mathbf{H} = \mathbf{Q} \mathbf{S}^{1/2}$  with  $\mathbf{Q}$  orthonormal and  $\mathbf{S}$  positive diagonal, and its noise model  $\Sigma = \sigma \mathbf{I} + \mathbf{H} \mathbf{D} \mathbf{H}^T$  with  $\mathbf{D}$  diagonal. Rewriting the latter  $\Sigma = \mathbf{Q}_{\perp} (\sigma \mathbf{I}) \mathbf{Q}_{\perp}^T + \mathbf{Q} \mathbf{S}^{1/2} (\mathbf{D} + \sigma \mathbf{S}^{-1}) \mathbf{S}^{1/2} \mathbf{Q}^T$ , and identifying  $\mathbf{S}^{1/2} \equiv \mathbf{R}$ ,  $\mathbf{D} + \sigma \mathbf{S}^{-1} \equiv \tilde{\mathbf{D}}$  and

<sup>2</sup>For a parametrization of orthonormal matrices, see for instance this of Lezcano Casado [2019]) implemented in pytorchPaszke et al. [2019].

$\sigma\mathbf{I} \equiv \tilde{\mathbf{B}}$ , we see that the OILMM is a special case of our model, where  $\mathbf{R}$  is constrained to be positive diagonal instead of triangular,  $\mathbf{M}$  is zero and  $\tilde{\mathbf{B}}$  is scalar instead of diagonal. The GPPCA (Gu and Shen [2020]) is an OILMM model further restricted to have a scalar  $\Sigma$ . The restriction on  $\mathbf{R}$  is likely to be the most significant; we study the effect of these various simplifications in the next experimental section.

## 5 Experimental results

### 5.1 Tested models

We compare our PLMC to several baselines : a state-of-the art ICM model, a state-of-the art variational LMC, and the OILMM - which in fact is only a subcase of PLMC as explained in remark 5. We also wish to **test several possible implementations and simplifications of the projected model**, as mentioned in remark 4. We therefore end up with 7 models to test: `ICM` (LMC with a shared kernel between latent processes and algebra tricks - see Rakitsch et al. [2013]), `var` (variational LMC as described in Hensman et al. [2015] and implemented in `gpytorch` (Gardner et al. [2018]), with a Cholesky variational distribution and a number  $\lfloor n/1.5 \rfloor$  of learned inducing points<sup>3</sup>), `proj` (fully parametrized PLMC with dense matrix  $\tilde{\mathbf{B}}$ ), `diagproj` (PLMC with diagonal  $\tilde{\mathbf{B}}$ , theoretically equivalent to the latter - see prop.11), `bdn` (PLMC with  $\mathbf{M} = \mathbf{0}$ ), `bdn_diag` (PLMC with  $\mathbf{M} = \mathbf{0}$  and diagonal  $\tilde{\mathbf{B}}$ ) and `oilmm` (PLMC with positive diagonal  $\mathbf{R}$ , scalar  $\tilde{\mathbf{B}}$  and  $\mathbf{M} = \mathbf{0}$ ). Unless otherwise specified, `LMC`, `ICM` and `var` models are implemented with a fully general gaussian likelihood, putting no constraint on their  $\Sigma$  matrix. The training protocol for each model (optimizer, learning rate schedule, number of iterations, initialization, stopping criterion...) was hand-refined and finally taken identical for all of them, as the chosen common scheme yielded near-optimal convergence for all; it is specified in Annex D.

<sup>3</sup>Picking a larger number of learned inducing points or even putting fixed inducing points at all observed locations, although theoretically more accurate, proved less stable in practice.

### 5.2 Synthetic data

**Data description.** We start with a parametric study on synthetic data, in order to explore the effect of some data properties on our models. It is generated according to a univariate LMC model: its latent processes are defined by  $q$  1D Matern kernels ( $\nu = 2.5$ ) with lengthscales equidistant in the interval  $[l_{min}, l_{max}]$ , and sampled at the locations  $\mathbf{X}_{train}$  ( $n$  points equidistant in  $[-1, 1]$ ) and  $\mathbf{X}_{test}$  (2500 points sampled uniformly in the same interval). The coefficients of the mixing matrix  $\mathbf{H}$  are sampled from independant normal distribution  $\mathcal{N}(0, 1)$ . After latent signals are mixed, structured noise is added in a manner inspired from Rakitsch et al. [2013]: a parameter  $\mu_{noise}$  controls the signal-to-noise proportion ( $\mathbf{Y}_{full} = \mu_{noise} \mathbf{Y}_{noise} + (1 - \mu_{noise}) \mathbf{Y}_{signal}$ ), and another  $\mu_{str}$  rules the proportion of structured-to-unstructured noise ( $\mathbf{Y}_{noise} = \mu_{str} \mathbf{Y}_{noise}^{str} + (1 - \mu_{str}) \mathbf{Y}_{noise}^{ind}$ ).  $\mathbf{Y}_{noise}^{str}$  is obtained by the mixing of  $q_{noise}$  white noise processes by a matrix  $\mathbf{H}_{noise}$ , generated in the same way as  $\mathbf{H}$ , while  $\mathbf{Y}_{noise}^{ind}$  is simply the concatenation of  $p$  independant white noises. The noise thus contains a part that is correlated over all tasks, and one that is specific to each task. Overall the synthetic data is described by 8 parameters; when they are not varied for an experiment or explicitly specified, their fixed values are the following:  $p = 100$ ,  $q = 25$ ,  $q_{noise} = 25$ ,  $n = 500$ ,  $\mu_{noise} = 0.1$ ,  $\mu_{str} = 0.9$ ,  $l_{min} = 0.01$  and  $l_{max} = 0.5$ .

All tests are run  $N_{rep}$  times with data generated from as many random seeds, and resulting metrics are averaged. For all models, the chosen kernel type and number of latent processes are always this of the data (no model misspecification). In the following graphs, models `proj` and `bdn` are omitted, as by prop.11 they are theoretically equivalent to models `diagproj` and `bdn_diag` respectively; this equivalence will be tested later.

**DPN condition severity.** The first and main observation is that *projected models overall perform as good or better as the baselines*, even in setups where high-magnitude structured noise should handicap them. This way, figure 1 shows that for the highest noise magnitudes ( $\mu_{noise} \simeq 0.5$ , corresponding to

a signal-to-noise ratio of 1) and a highly-structured noise ( $\mu_{str} = 0.99$ ), the RMSEs of the projected models `diagproj` and `bdn_diag` are as low as these of their ICM and variational counterparts: in fact, all of them follow the expected asymptote  $Err_{L1} \simeq \mu_{noise}$ . Before this asymptote, ICM and OILMM seem to be struggling. The same is observed when varying  $\mu_{str}$  (figure 2) or  $q_{noise}$  (not displayed): **projected models don't suffer disproportionately from complex noise structure in the data**. Interestingly, model `bdn_diag` seems to be the most robust to it, even though an additional constraint is imposed on its noise model (the BDN assumption 2).

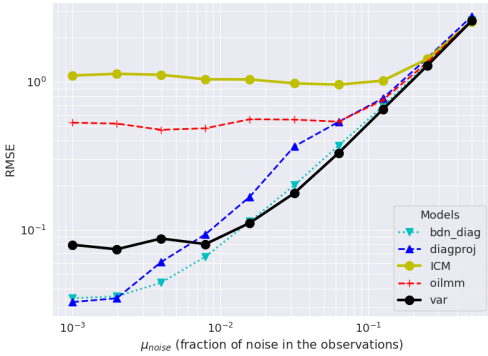


Figure 1: RMSE of several models for increasing data noise magnitude, with highly structured noise ( $\mu_{str} = 0.99$ ). Averaged over  $N_{rep} = 40$  random datasets

However, the impact of noise model assumptions on variance estimation is slightly larger. We measure the quality of variance estimation through Predictive Variance Adequacy, which assesses whether the predictive distribution has the right width:  $PVA = \frac{1}{p} \sum_{j=1}^p \log \left( \frac{1}{n} \sum_{i=1}^n \frac{(y_{ij} - \hat{y}_{ij})^2}{\hat{v}_{ij}} \right)$ , with  $y_{ij}$  the true value of output  $j$  at point  $i$ ,  $\hat{y}_{ij}$  the corresponding estimated value and  $\hat{v}_{ij}$  the corresponding predicted variance. Its optimal value is 0, in which case the predicted variance is equal to the observed deviation at each point and task. Figure 3 shows that for projected models, the higher the number of noise latent processes, the further PVA departs from its optimal value - a behavior not observed for the variational

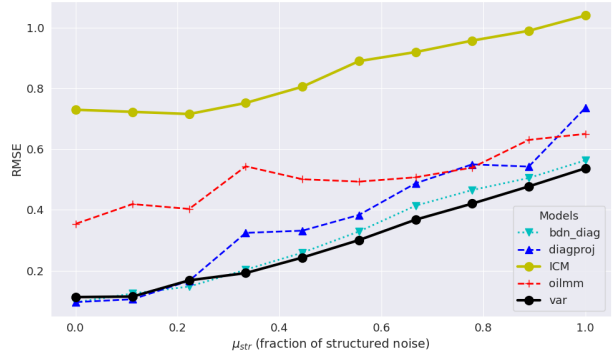


Figure 2: RMSE of several models for increasing proportion of structured noise, with fixed noise magnitude  $\mu_{noise} = 0.1$ . Averaged over  $N_{rep} = 20$  random datasets

model <sup>4</sup>. Yet increasing noise magnitude via  $\mu_{noise}$  or noise cross-correlations via  $\mu_{str}$  doesn't reproduce this phenomenon: all PVA values then remain very close to zero <sup>5</sup>.

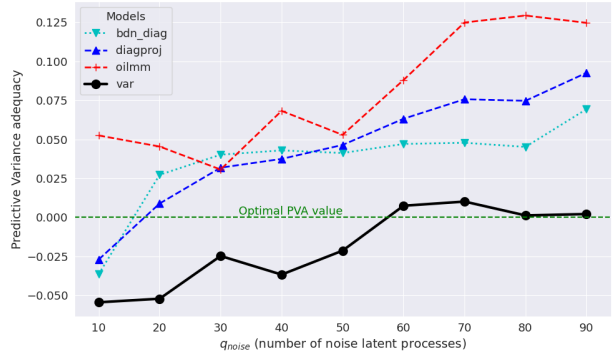


Figure 3: Average Predictive Variance Adequacy of several models for increasing number of noise latent processes  $q_{noise}$ , with  $\mu_{noise} = 0.1$ ,  $\mu_{str} = 0.9$ , and  $N_{rep} = 10$ .

<sup>4</sup>This experiment could also not be performed on the ICM model, because `pytorch` implementation made variance estimation impossible for this data size.

<sup>5</sup>Surprisingly, it is at low values of  $\mu_{noise}$  and  $\mu_{str}$  that PVA gets worse, and this for all models.



**Training duration.** Figure 4 plotting training duration against the number of tasks – for a fixed number of latent processes – yields two important observations: **training PLMCs to convergence takes a time similar to that of the variational model;** and second, **these training times don’t increase with the number of tasks (between 50 and 200 tasks)**. This was expected for PLMCs and the `var` model, as the relevant quantity in this case is rather the number of latent processes, which all computations scale linearly in; it is more surprising for the ICM, and indicates that other computational expenses are at play. The negative relation between  $t_{train}$  and  $p$  on the left-hand side of the graph stems from the training protocol, described in Annex D: models are trained until a convergence criterion is met, not in a fixed budget of iterations. More observations regarding training duration are presented in Annex E.

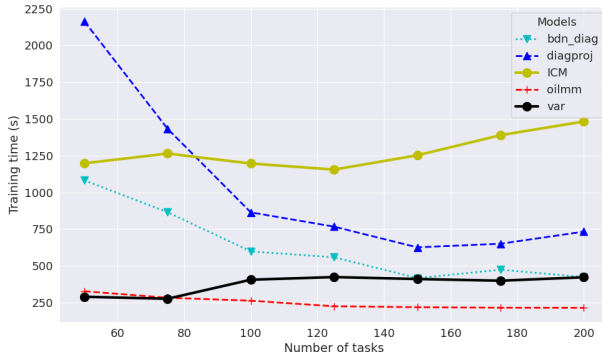


Figure 4: Training duration of several models for increasing number of tasks and a fixed number  $q = 25$  of latent processes. Averaged over  $N_{rep} = 20$  random datasets

**Other observations.** All models didn’t respond in the same way to an increase in  $p$  with fixed  $q$ , or conversely to an increase in  $q$  with fixed  $p$ : in our experiments, the accuracies of `var`, `bdn` and `bdn_diag` were insensitive to these variations, whereas for other PLMCs and ICM the RMSE could vary by  $\pm 50\%$ , as a function of both the ratio between  $p$  and  $q$  and their

absolute values. The corresponding graphs are available in Annex E. Otherwise, altering the other data parameters (modifying the number of training points, reducing the range of kernel lengthscales...) offered very little discriminative power over all models.

### 5.3 Real data

In the two following experiments, we used a Matérn-5/2 kernel with input-specific parametrized lengthscales for all models. A full-rank gaussian likelihood (general  $\Sigma$  matrix) was tried for `var` and ICM models, but only retained for `var`: the ICM performed slightly to much better with independent task noises (diagonal  $\Sigma$ ). Results display the metric  $Q_{L1}^{95}$ , which is simply the quantile of L1 errors at level 95%, in the aim of assessing the occurrence of large errors. Two other experiments are presented in Annex E, with coherent results.

**SARCOS dataset.** We tested PLMCs on the well-known SARCOS dataset, described in Vijayakumar and Schaal [2000], which displays the dynamics of a robot arm (position, speed and acceleration of its 7 articulation points) and the corresponding torque commands for these articulations. The goal is to modelize the inverse dynamics, that is, to infer the torque commands (7 outputs) from the dynamic measurements (21 features). The dataset contains about 45 000 points corresponding to various movements sampled at 100Hz; for ease of computation, we subsampled it at 10Hz. We respected the train/test split of Rasmussen and Williams [2006]. Output features were centered and normalized by their standard deviation. Even after subsampling, the problem remained too large to reach a reasonable computation time; **we therefore wrapped latent processes of PLMCs with an inducing points approximation**, as suggested in remark 2. We adopted the approach of Titsias [2009], once again implemented in `gpytorch`. We also wrapped the ICM model in this way, and selected an identical number of inducing points  $N_{ind} = 500$  for all models (including `var`). Tests were run for  $q$  ranging from 1 to 7, and the best accuracy was reached for  $q = 7$  for all models. Results are displayed in table 1 below: PLMCs outperform all baselines both in

accuracy and computation time, including `var` model which severely underperforms in this case (except for variance estimation).

Table 1: Experimental results on dataset SARCOS.

Model	$N_{iter}$	$t_{train}$	RMSE	$Q_{L1}^{95}$	PVA
proj	4485	193	0.102	0.215	-1.46
diagproj	4485	191	0.102	0.215	-1.46
bdn	4570	183	0.102	0.214	-1.45
bdn_diag	4539	180	0.103	0.216	-1.44
oilmm	4446	174	0.104	0.218	-1.42
ICM	7997	45846	0.147	0.305	-2.51
var	2336	861	0.629	1.369	-0.31

**Neutronics dataset.** This dataset consists in so-called *homogenized cross-sections* (dubbed HXS), nuclear data that has already been processed by physics codes to be used in a full-size reactor core simulation – see e.g Szames [2020]. The objective is one of surrogate modeling: rather than generating HXS’s on-the-fly, reactor core simulators interpolate their tabulated values. Inputs correspond to reactor operation parameters (fuel temperature, depletion of fissile material...). The resulting dataset contains 4 features, 287 outputs and 201 input points. Outputs were centered and normalized by their maximal absolute value. Models are defined as before, with  $\lfloor n/1.5 \rfloor$  inducing points for the `var` model (see section 5.1), and 20 latent functions for each, a number found to be near-optimal for all <sup>6</sup>. Results are displayed in table 2. These very low RMSE values obtained on unit-sized outputs are not abnormal: the data is of small effective linear dimension (i.e outputs are strongly correlated), virtually noiseless, and very smooth. One PLMC (`bdn`) matches the accuracy of the `var` model, and outperforms OILMM and ICM; `bdn_diag` is nearly as good. They also yield better variance estimation, as measured by PVA (the optimum being 0). However, their convergence was much longer to reach (as measured by the number of necessary iterations), resulting in larger training times.

<sup>6</sup>In fact, the data being of very low effective dimension, all values of  $q$  between 20 and 40 yield about the same results.

Table 2: Experimental results on the neutronics dataset.

Model	$N_{iter}$	$t_{train}$	RMSE	$Q_{L1}^{95}$	PVA
proj	49241	2299	0.0084	0.0182	-0.36
diagproj	53387	1193	0.0033	0.0077	-0.81
bdn	27121	521	0.0016	0.0032	-1.45
bdn_diag	56115	1057	0.0022	0.0046	-1.60
oilmm	11103	393	0.0038	0.0072	-1.45
ICM	16082	479	0.0018	0.0036	-5.47
var	11936	463	0.0016	0.0031	-5.83

### PLMC parametrization and simplification.

The presented experiments give some insight about two questions we asked before: is the theoretical equivalence between `proj` and `diagproj` parametrizations, corresponding respectively to a triangular or diagonal matrix for the root of  $\tilde{\mathbf{B}}$  (see prop. 11), verified in practice? And is the BDN assumption (see prop.2) impactful on the quality of predictions? The evidence amassed so far answers both question in the negative. Substantial discrepancy is observed between `proj` and `diagproj` models (resp. between `bdn` and `bdn_diag`) in the neutronics experiment, as in several other in Annex E or not presented here, and **gaps are almost always in favor of the diagonal parametrization**, which probably benefits from its lesser number of parameters. Much more surprisingly, in addition to providing the expected speed-up, **the BDN assumption seems to increase prediction accuracy rather than hindering it**; even the effect on variance estimation is ambiguous, clearly negative in the neutronics experiment but slightly positive in the synthetic one. The interaction of these two modeling choices is also non-trivial, as it can be seen in table 2: enforcing a diagonal  $\tilde{\mathbf{B}}$  has a positive effect, enforcing the BDN assumption too, yet combining both is slightly detrimental (`bdn_diag` performs worse than `bdn`). These modeling choices should therefore remain open for the time being, though both simplifications appear globally beneficial.

## 6 Conclusion

In this article, we showed that the equations of the Linear Model of Co-regionalization could be reformulated in a way that reveals its low-rank latent structure. These expressions have the striking property – first observed Bruinsma et al. [2020] – of decoupling if and only if a certain condition on the noise is verified, enabling computation to be linear in the number of latent processes rather than cubic in the number of tasks. We gave a general parametrization of LMC models enforcing this noise assumption and optimized the marginal likelihood accordingly, thus bringing out a new model dubbed as *Projected LMC* (PLMC). We tested this model on real and synthetic data, comparing several possible implementations between them and with concurrent approaches, and studying their behavior as data parameters vary. PLMCs showed themselves to compete very well with state-of-the-art variational LMC, even in setups where they should theoretically be challenged (large and highly-structured noises). We exhibited an approximation of the model which seems to have little effect on prediction quality while making the model simpler, lighter in parameters, more robust and significantly faster.

In addition to yielding theoretical insights (see for instance Annex H for a comparison of the approximations made by several LMC models), the PLMC appears as a viable and more straightforward alternative to its variational counterparts, in particular in applications where the inducing points approximation enforced by the latter is not desired. It makes the LMC framework scalable in the number of tasks, without however addressing scalability in the number of input points<sup>7</sup>. It can be implemented as a mere overlay of a batch single-output GP, by parametrizing a mixing matrix and adding a few simple extra terms to the likelihood. Its exact GP treatment also authorizes operations which are more cumbersome with variational methods, such as leave-one-out error computation (Rasmussen and Williams [2006]) and incorporation of new observations, (Jiang et al. [2020]),

<sup>7</sup>Yet we showed in remark 2 how existing approximations could easily be plugged onto it to fix this issue.

ultimately facilitating the use of gaussian processes for multitask optimization and adaptive sampling.

## References

- Mauricio A. Alvarez, Lorenzo Rosasco, and Neil D. Lawrence. Kernels for vector-valued functions: A review. *Foundations and Trends in Machine Learning*, 4(3):195–266, 2012. ISSN 1935-8237. doi: 10.1561/22000000036. URL <http://dx.doi.org/10.1561/22000000036>.
- Ilias Bilionis, Nicholas Zabaras, Bledar A. Konomi, and Guang Lin. Multi-output separable gaussian process: Towards an efficient, fully bayesian paradigm for uncertainty quantification. *Journal of Computational Physics*, 241:212–239, 2013. ISSN 0021-9991. doi: <https://doi.org/10.1016/j.jcp.2013.01.011>. URL <https://www.sciencedirect.com/science/article/pii/S0021999113000417>.
- Christopher M. Bishop. *Pattern recognition and machine learning*. Information science and statistics. Springer, 2006. ISBN 978-0-387-31073-2.
- Edwin V Bonilla, Kian Chai, and Christopher Williams. Multi-task gaussian process prediction. In J. Platt, D. Koller, Y. Singer, and S. Roweis, editors, *Advances in Neural Information Processing Systems*, volume 20. Curran Associates, Inc., 2007. URL [https://proceedings.neurips.cc/paper\\_files/paper/2007/file/66368270ffd51418ec58bd793f2d9b1b-Paper.pdf](https://proceedings.neurips.cc/paper_files/paper/2007/file/66368270ffd51418ec58bd793f2d9b1b-Paper.pdf).
- Edwin V Bonilla, Karl Krauth, and Amir Dezfouli. Generic inference in latent gaussian process models. *J. Mach. Learn. Res.*, 20:117–1, 2019.
- Stephen P Boyd and Lieven Vandenberghe. *Convex optimization*. Cambridge university press, 2004.
- Wessel Bruinsma, Eric Perim, Will Tebbutt, Scott Hosking, Arno Solin, and Richard Turner. Scalable exact inference in multi-output gaussian processes. In Hal Daume and Aarti Singh, editors, *ICML’20: Proceedings of the 37th International Conference on Machine Learning*, 2020.

- Andrea Coraddu, Luca Oneto, Alessandro Ghio, Stefano Savio, Davide Anguita, and Massimo Figari. Machine learning approaches for improving condition-based maintenance of naval propulsion plants. *Journal of Engineering for the Maritime Environment*, –(–):–, 2014.
- Astrid Dahl and Edwin V Bonilla. Grouped gaussian processes for solar power prediction. *Machine Learning*, 108(8-9):1287–1306, 2019.
- Jacob R Gardner, Geoff Pleiss, David Bindel, Kilian Q Weinberger, and Andrew Gordon Wilson. Gpytorch: Blackbox matrix-matrix gaussian process inference with gpu acceleration. In *Advances in Neural Information Processing Systems*, 2018.
- Mengyang Gu and Weining Shen. Generalized probabilistic principal component analysis of correlated data. *The Journal of Machine Learning Research*, 21(1):428–468, 2020.
- James Hensman, Alexander Matthews, and Zoubin Ghahramani. Scalable Variational Gaussian Process Classification. In Guy Lebanon and S. V. N. Vishwanathan, editors, *Proceedings of the Eighteenth International Conference on Artificial Intelligence and Statistics*, volume 38 of *Proceedings of Machine Learning Research*, pages 351–360, San Diego, California, USA, 09–12 May 2015. PMLR. URL <https://proceedings.mlr.press/v38/hensman15.html>.
- Neil Houlsby, Ferenc Huszar, Zoubin Ghahramani, and Jose Hernández-lobato. Collaborative gaussian processes for preference learning. In F. Pereira, C.J. Burges, L. Bottou, and K.Q. Weinberger, editors, *Advances in Neural Information Processing Systems*, volume 25. Curran Associates, Inc., 2012. URL [https://proceedings.neurips.cc/paper\\_files/paper/2012/file/afdec7005cc9f14302cd0474fd0f3c96-Paper.pdf](https://proceedings.neurips.cc/paper_files/paper/2012/file/afdec7005cc9f14302cd0474fd0f3c96-Paper.pdf).
- Shali Jiang, Daniel Jiang, Maximilian Balandat, Brian Karrer, Jacob Gardner, and Roman Garnett. Efficient nonmyopic bayesian optimization via one-shot multi-step trees. In H. Larochelle, M. Ranzato, R. Hadsell, M.F. Balcan, and H. Lin, editors, *Advances in Neural Information Processing Systems*, volume 33, pages 18039–18049. Curran Associates, Inc., 2020. URL [https://proceedings.neurips.cc/paper\\_files/paper/2020/file/d1d5923fc822531bbfd9d87d4760914b-Paper.pdf](https://proceedings.neurips.cc/paper_files/paper/2020/file/d1d5923fc822531bbfd9d87d4760914b-Paper.pdf).
- Mario Lezcano Casado. Trivializations for gradient-based optimization on manifolds. In H. Wallach, H. Larochelle, A. Beygelzimer, F. d'Alché-Buc, E. Fox, and R. Garnett, editors, *Advances in Neural Information Processing Systems*, volume 32. Curran Associates, Inc., 2019. URL [https://proceedings.neurips.cc/paper\\_files/paper/2019/file/1b33d16fc562464579b7199ca3114982-Paper.pdf](https://proceedings.neurips.cc/paper_files/paper/2019/file/1b33d16fc562464579b7199ca3114982-Paper.pdf).
- Haitao Liu, Jianfei Cai, and Yew-Soon Ong. Remarks on multi-output gaussian process regression. *Knowledge-Based Systems*, 144:102–121, 2018. ISSN 0950-7051. doi: <https://doi.org/10.1016/j.knosys.2017.12.034>. URL <https://www.sciencedirect.com/science/article/pii/S0950705117306123>.
- Haitao Liu, Yew-Soon Ong, Xiaobo Shen, and Jianfei Cai. When gaussian process meets big data: A review of scalable gps. *IEEE Transactions on Neural Networks and Learning Systems*, 31(11):4405–4423, 2020. doi: 10.1109/TNNLS.2019.2957109.
- Haitao Liu, Jiaqi Ding, Xinyu Xie, Xiaomo Jiang, Yusong Zhao, and Xiaofang Wang. Scalable multi-task gaussian processes with neural embedding of coregionalization. *Knowledge-Based Systems*, 247:108775, 2022. ISSN 0950-7051. doi: <https://doi.org/10.1016/j.knosys.2022.108775>. URL <https://www.sciencedirect.com/science/article/pii/S0950705122003641>.
- Haitao Liu, Kai Wu, Yew-Soon Ong, Chao Bian, Xiaomo Jiang, and Xiaofang Wang. Learning multitask gaussian process over heterogeneous input domains. *IEEE Transactions on Systems, Man, and Cybernetics: Systems*, 53(10):6232–6244, 2023. doi: 10.1109/TSMC.2023.3281973.

- Ilya Loshchilov and Frank Hutter. Decoupled weight decay regularization. *arXiv preprint arXiv:1711.05101*, 2017.
- Wesley J Maddox, Maximilian Balandat, Andrew G Wilson, and Eytan Bakshy. Bayesian optimization with high-dimensional outputs. In M. Ranzato, A. Beygelzimer, Y. Dauphin, P.S. Liang, and J. Wortman Vaughan, editors, *Advances in Neural Information Processing Systems*, volume 34, pages 19274–19287. Curran Associates, Inc., 2021. URL [https://proceedings.neurips.cc/paper\\_files/paper/2021/file/a0d3973ad100ad83a64c304bb58677dd-Paper.pdf](https://proceedings.neurips.cc/paper_files/paper/2021/file/a0d3973ad100ad83a64c304bb58677dd-Paper.pdf).
- Adam Paszke, Sam Gross, Francisco Massa, Adam Lerer, James Bradbury, Gregory Chanan, Trevor Killeen, Zeming Lin, Natalia Gimelshein, Luca Antiga, Alban Desmaison, Andreas Kopf, Edward Yang, Zachary DeVito, Martin Raison, Alykhan Tejani, Sasank Chilamkurthy, Benoit Steiner, Lu Fang, Junjie Bai, and Soumith Chintala. Pytorch: An imperative style, high-performance deep learning library. In H. Wallach, H. Larochelle, A. Beygelzimer, F. d'Alché-Buc, E. Fox, and R. Garnett, editors, *Advances in Neural Information Processing Systems*, volume 32. Curran Associates, Inc., 2019. URL [https://proceedings.neurips.cc/paper\\_files/paper/2019/file/bdbca288fee7f92f2bfa9f7012727740-Paper.pdf](https://proceedings.neurips.cc/paper_files/paper/2019/file/bdbca288fee7f92f2bfa9f7012727740-Paper.pdf).
- K. B. Petersen and M. S. Pedersen. The matrix cookbook, nov 2012. URL <http://www2.compute.dtu.dk/pubdb/pubs/3274-full.html>. Version 20121115.
- Barbara Rakitsch, Christoph Lippert, Karsten Borgwardt, and Oliver Stegle. It is all in the noise: Efficient multi-task gaussian process inference with structured residuals. In C.J. Burges, L. Bottou, M. Welling, Z. Ghahramani, and K.Q. Weinberger, editors, *Advances in Neural Information Processing Systems*, volume 26. Curran Associates, Inc., 2013. URL [https://proceedings.neurips.cc/paper\\_files/paper/2013/file/59c33016884a62116be975a9bb8257e3-Paper.pdf](https://proceedings.neurips.cc/paper_files/paper/2013/file/59c33016884a62116be975a9bb8257e3-Paper.pdf).
- Carl Edward Rasmussen and Christopher K. I. Williams. *Gaussian processes for machine learning*. Adaptive computation and machine learning. MIT Press, 2006. ISBN 978-0-262-18253-9. OCLC: ocm61285753.
- Esteban Alejandro Szames. *Few group cross section modeling by machine learning for nuclear reactor*. PhD thesis, 2020. URL <http://www.theses.fr/2020UPASS134>.
- Zhe Tang, Sihao Li, Kyeong Soo Kim, and Jeremy Smith. Multi-output gaussian process-based data augmentation for multi-building and multi-floor indoor localization. *2022 IEEE International Conference on Communications Workshops (ICC Workshops)*, pages 361–366, 2022. doi: 10.1109/ICCWorkshops53468.2022.9814616.
- Yee Whye Teh, Matthias Seeger, and Michael I. Jordan. Semiparametric latent factor models. In Robert G. Cowell and Zoubin Ghahramani, editors, *Proceedings of the Tenth International Workshop on Artificial Intelligence and Statistics*, volume R5 of *Proceedings of Machine Learning Research*, pages 333–340. PMLR, 06–08 Jan 2005. URL <https://proceedings.mlr.press/r5/teh05a.html>. Reissued by PMLR on 30 March 2021.
- Michalis Titsias. Variational learning of inducing variables in sparse gaussian processes. In David van Dyk and Max Welling, editors, *Proceedings of the Twelfth International Conference on Artificial Intelligence and Statistics*, volume 5 of *Proceedings of Machine Learning Research*, pages 567–574, Hilton Clearwater Beach Resort, Clearwater Beach, Florida USA, 16–18 Apr 2009. PMLR. URL <https://proceedings.mlr.press/v5/titsias09a.html>.
- Sethu Vijayakumar and Stefan Schaal. Locally weighted projection regression: An  $o(n)$  algorithm for incremental real time learning in high dimensional space. In *Proceedings of the seventeenth international conference on machine learning (ICML*

2000), volume 1, pages 288–293. Morgan Kaufmann, 2000.

Yan Wen, Guoli Li, Qunjing Wang, Xiwen Guo, and Wenping Cao. Modeling and analysis of permanent magnet spherical motors by a multitask gaussian process method and finite element method for output torque. *IEEE Transactions on Industrial Electronics*, 68(9):8540–8549, 2021. doi: 10.1109/TIE.2020.3018078.

Andrew Wilson and Ryan Adams. Gaussian process kernels for pattern discovery and extrapolation. In Sanjoy Dasgupta and David McAllester, editors, *Proceedings of the 30th International Conference on Machine Learning*, volume 28 of *Proceedings of Machine Learning Research*, pages 1067–1075, Atlanta, Georgia, USA, 17–19 Jun 2013. PMLR. URL <https://proceedings.mlr.press/v28/wilson13.html>.

Renhui Zhang and Xutao Zhao. Inverse method of centrifugal pump blade based on gaussian process regression. *Mathematical Problems in Engineering*, 2020:1–10, 2020.

Exact and general decoupled solutions of the LMC Multitask Gaussian Process model  
(Supplementary Material)

## A CODE

Model implementation and experiments are available at <https://github.com/QWERTY6191/projected-lmc>.

## B Model implementation

In this section we give a few additional details about implementation of the PLMC. Model parametrization has already be detailed in section 4.2.

**Inference.** To make predictions with the model, we perform the following steps (written here for a single test point – we wish to compute  $p(\hat{\mathbf{y}}_*|\mathbf{Y}) = \mathbf{f}(x_*)$ ):

1. Compute the projection matrix  $\mathbf{T}$  from model parameters with the expression of prop. 9:  $\mathbf{T} = \mathbf{R}^{-1}\mathbf{Q}^T + \Sigma_{\mathbf{P}}\mathbf{M}\mathbf{Q}_{\perp}^T$ . The second term is not computed if  $\mathbf{M} = \mathbf{0}$  (BDN assumption)
2. Compute the projected data  $\mathbf{T}\mathbf{Y}$ . These two steps can be performed in the opposite order; in particular, computing  $\mathbf{R}^{-1}\mathbf{Q}^T\mathbf{Y}$  can be done by computing  $\mathbf{Q}^T\mathbf{Y}$  first, then solving for  $\mathbf{X}$  the Cholesky system  $\mathbf{R}\mathbf{X} = \mathbf{Q}^T\mathbf{Y}$ .
3. Set the training labels of the GP model representing latent processes to  $\mathbf{T}\mathbf{Y}$ . If this GP implementation stores caches, as it is often the case, one should verify that they are correctly updated.
4. Compute posteriors of the latent processes with expressions 6 :  $p(\hat{u}_{i_*}|\mathbf{Y}) = \mathcal{N}(\mathbf{k}_{i_*}^T(\mathbf{K}_i + \sigma_i^2\mathbf{I}_n)^{-1}\mathbf{T}_i\mathbf{Y}, k_{i_*} - \mathbf{k}_{i_*}^T(\mathbf{K}_i + \sigma_i^2\mathbf{I}_n)^{-1}\mathbf{k}_{i_*})$ . Once again, these are standard GP expressions which can be solved with any GP implementation, including approximated ones.
5. Compute the noise matrix  $\Sigma$  from model parameters. This is done via its additive decomposition, such as depicted in corollary 1 :  $\Sigma = \mathbf{Q}\mathbf{R}\tilde{\mathbf{D}}\mathbf{R}^T\mathbf{Q}^T + \mathbf{Q}_{\perp}\tilde{\mathbf{B}}\mathbf{Q}_{\perp}^T + 2\text{Sym}(\mathbf{Q}\mathbf{R}\tilde{\mathbf{M}}\mathbf{Q}_{\perp}^T)$ .  $\tilde{\mathbf{D}}$  and  $\tilde{\mathbf{B}}$  are computed by block-matrix inversion formulas, like it is done in the proof F.2 of prop.8 :  $\tilde{\mathbf{D}} = \Sigma_{\mathbf{P}} + \Sigma_{\mathbf{P}}\mathbf{M}\tilde{\mathbf{B}}\mathbf{M}^T\Sigma_{\mathbf{P}}$  and  $\tilde{\mathbf{M}} = -\Sigma_{\mathbf{P}}\mathbf{M}\tilde{\mathbf{B}}$ .
6. Combine latent estimators with the mixing matrix and add the noise:  $p(\hat{\mathbf{y}}_*|\mathbf{Y}) = \mathcal{N}(\mathbf{H}\mathbb{E}(\hat{\mathbf{u}}_*|\mathbf{Y}), \mathbf{H}\mathbb{V}(\hat{\mathbf{u}}_*|\mathbf{Y})\mathbf{H}^T + \Sigma)$ . If only the diagonal of the covariance is needed, we can retrieve it through the expression  $\mathbb{V}(\hat{\mathbf{y}}_*|\mathbf{Y}) = (\mathbf{H} \odot \mathbf{H})\mathbb{V}(\hat{\mathbf{u}}_*|\mathbf{Y}) + \text{diag}(\Sigma)$ , with  $\odot$  the Hadamard product.

Of course, items 1, 2 and 5 can be precomputed and cached as long as model parameters are kept constant.

**Likelihood computation.** To compute the loss (marginal log-likelihood) during a training iteration, perform the following steps.

1. Compute the projection matrix  $\mathbf{T}$  from model parameters (same as for inference)

2. Compute the projected data  $\mathbf{T}\mathbf{Y}$  (same as for inference)
3. Set the training labels of the GP model representing latent processes to  $\mathbf{T}\mathbf{Y}$  (same as for inference)
4. Compute the MLL of latent processes:  $\log p(\mathbf{U}_i) = \log \mathcal{N}(\mathbf{T}_i\mathbf{Y}|\mathbf{0}, \mathbf{K}_i + \sigma_i\mathbf{I}_n)$  This is a standard GP expression which can be solved with any GP implementation, including approximated ones.
5. Sum these likelihood terms and add the regularisation terms (representing data and noise lost by projection), easily computed from model parameters, to obtain the full MLL of prop. 10:  $-2 \log p(\mathbf{Y}) = (p-q)n \log 2\pi + 2n \log |\mathbf{R}| + n \log |\tilde{\mathbf{B}}| + \text{Tr}(\mathbf{Y}^T \mathbf{Q}_\perp \tilde{\mathbf{B}}^{-1} \mathbf{Q}_\perp^T \mathbf{Y}) + \sum_{i=1}^q \log \mathcal{N}(\mathbf{T}_i\mathbf{Y}|\mathbf{0}, \mathbf{K}_i + \sigma_i\mathbf{I}_n)$ . Remember (see section 4.2) that  $\tilde{\mathbf{B}}^{-1}$  should be parametrized by its Cholesky decomposition  $\tilde{\mathbf{B}}^{-1} = \mathbf{L}\mathbf{L}^T$  (and  $\mathbf{L}$  can eventually be enforced to be diagonal by prop. 11), so that  $\mathbf{Y}^T \mathbf{Q}_\perp \tilde{\mathbf{B}}^{-1} \mathbf{Q}_\perp^T \mathbf{Y} = \mathbf{N}\mathbf{N}^T$  with  $\mathbf{N} = \mathbf{Y}^T \mathbf{Q}_\perp \mathbf{L}$ .

## C Computational complexities

We here compare the computational complexities, both in time and memory space, of inference and MLL computation for all models considered in this article. References for the stated values are given in the last column of table 3. For inference, we make the distinction between computation of caches (inverse kernel matrices, projection matrix...) which values are independent of test points and can thus be precomputed, and test-dependent values themselves. We also denote by  $m$  the number of inducing points for the variational model; we recall that the variational approach considered here is this of Hensman et al. [2015].

Table 3: Computational complexities of several models.

Model	Time (inference)	Memory (inference)	Time (inf. caches)	Memory (inf. caches)	Time (MLL)	Memory (MLL)	References
PLMC (without BDN assumption)	$O(pq)$	$O(pq)$	$O(qn^3 + p(p-q)n)$	$O(qn^2)$	$O(qn^3 + p^3)$	$O(qn^2 + p^2)$	-
PLMC (with BDN assumption)	$O(pq)$	$O(pq)$	$O(qn^3 + pqn)$	$O(qn^2)$	$O(qn^3 + p^3)$	$O(qn^2 + p^2)$	-
OILMM	$O(pq)$	$O(pq)$	$O(qn^3 + pqn)$	$O(qn^2)$	$O(qn^3 + pq^2)$	$O(qn^2 + pq)$	Bruinsma et al. [2020]
ICM	$O(pq)$	$O(pq)$	$O(n^3 + p^3)$	$O(n^2 + p^2)$	$O(n^3 + p^3)$	$O(n^2 + p^2)$	Rakitsch et al. [2013]
Variational	$O(pq)$	$O(pq)$	$O(qnm^2)$	$O(qm^2)$	$O(qnm^2)$	$O(qm^2)$	Hensman et al. [2015], Bonilla et al. [2019]

We can see that the main differences between models are:

- The effect of the inducing points approximation for the variational model: all kernel matrices of size  $n \times n$  are replaced by inducing points matrices of size  $m \times m$ , replacing all complexity terms in  $n^2$  by terms in  $m^2$ . Note that the same gains are achievable when coupling PLMCs with inducing points approximations.
- The presence of terms scaling like  $p$  in the computation of caches for PLMCs (which correspond to the projection of data) and ICM (corresponding to other operations), absent for the variational model.

We further note the difference in cache computation brought by the BDN assumption (term  $p(p-q)n$  replaced by  $pqn$ , with  $q \ll (p-q)$  in general), and the difference in MLL computation between OILMM and PLMCs (term  $pq^2$  replaced by  $p^3$ ): the latter is due to the necessity of parametrizing a full  $p \times p$  orthonormal matrix  $\mathbf{Q}_+$  rather than a  $p \times q$  one in OILMM. This difference, which could be a burden for applications with large  $p$ , could be alleviated by developing minibatch training for PLMC (with taskwise batches).



## D Experimental specifications

### D.1 Training protocol

For each model described in the main body of the article, the training dynamics were investigated individually on the synthetic data in order to verify that performance discrepancies weren't due to improper convergence. Modifications were tried out on the following items:

- The optimizer, between algorithms Adam, RAdam, NAdam, AdamW, SGD and LBFGS of the `torch.optim` package (Paszke et al. [2019]);
- The learning rate scheduler, between none, exponential decay, cosine annealing, and reduction upon arrival at a plateau (all implementations also taken from `torch.optim`);
- The maximal learning rate, over the range  $[10^{-3}; 10^{-1}]$ ;
- The maximal-to-minimal learning rate ratio, over a range of 1 to 100;
- The presence or absence of a stopping criterion, defined as an early stop when differences between consecutive values of the loss remain smaller (in relative value) to a given threshold  $\delta\mathcal{L}$  during a given number of iterations  $N_{patience}$ ;
- The values of  $\delta\mathcal{L}$  and  $N_{patience}$  if applicable;
- The (maximal) number of iterations  $N_{iter}^{max}$ , over the range  $[500; 10000]$ ;
- The initialization of the LMC coefficients<sup>8</sup>, between random sampling from i.i.d standard normal distributions, and setting  $\mathbf{Q}_+^{start} = \mathbf{V}$ ,  $\mathbf{R}_{start} = \mathbf{S}_{[1:q]}$  with  $\mathbf{Y} = \mathbf{USV}^T$  the SVD of the data.

All variations of the Adam optimizer performed about the same (for all models) and far better than the other optimizers, the best being AdamW (Loshchilov and Hutter [2017]) which was thus retained. Among schedulers, only absence of scheduling<sup>9</sup> and exponential learning rate decay yielded satisfactory results, and the latter was selected for its faster convergence and slightly higher precision at the end of training; the chosen value for the decay parameter was always  $\beta = \exp(\log(lr_{max}/lr_{min})/N_{iter}^{max})$ . Once these algorithms fixed, it appeared that for a rather large range of the remaining optimization parameters, the training loss converged monotonously for all models – with the occasional occurrence of a "jump" out of a minimal basin when the learning rate was too large or not decaying fast enough, quickly overcome if enough iterations remained. Optimization being monotonous, the suggested stopping criterion – training termination when no progress was made for a long time – proved to be a successful strategy, giving results as good or better as fixing a large number of iterations in advance. Choosing  $lr_{max} = 10^{-2}$ ,  $lr_{min} = 10^{-3}$ ,  $\delta\mathcal{L} = 10^{-4}$  and  $N_{patience}$  then yielded near-optimal accuracy for all models and was therefore adopted for all. Lastly, even when using the stopping criterion, a realistic maximal number of iterations had to be provided in order to compute the above learning rate decay factor  $\beta$ : experimentation revealed that model performances were very insensitive to this parameter, which mostly modulated convergence speed. In the same vein, in most cases the "clever" initialization of LMC coefficients with data-derived values was unnecessary to reach the global optimum but greatly sped up convergence. We therefore

---

<sup>8</sup>Initialization of other model parameters is much less problematic: all characteristic quantities of the toy data being of unit order, setting kernel parameters to  $\sim 1$  and noise parameters to  $\sim 10^{-2}$  always yields satisfactory results.

<sup>9</sup>Other than the automatic weight decay of the Adam optimizer.

chose to impose  $N_{iter}^{max} = 10000$  and SVD-based initialization for all models: the effective number of iterations provided by the stopping criterion thus became a metric to compare convergence speed between models.

Finally, we used a different learning rate policy for the experiments on the neutronics 5.3 and ship maintenance E datasets, because of the long convergence of some PLMCs in these cases: instead of an exponential scheduler, we applied the policy  $lr(i) = i/N_{max} * lr_{min}/lr_{max} + (N_{max} - i)/N_{max} * lr_{max}$  if  $i \leq N_{max}$  else  $lr_{min}/lr_{max}$  with  $i$  the current training iteration,  $lr_{min}$  and  $lr_{max}$  as before and  $N_{max} = 5000$ . This formula only corresponds to decreasing linearly from  $lr_{max}$  to  $lr_{min}$  in  $N_{max}$  iterations, then keeping a constant  $lr = lr_{min}$ . For the neutronics experiment, given the high achievable accuracy, we fixed a more demanding stopping criterion, setting the loss fluctuation threshold to  $\delta\mathcal{L} = 10^{-5}$ .

## D.2 Hardware specifications

The experiment behind figure 1, and real-data tests on neutronics, tidal height and ship maintenance datasets were performed on a 80-CPU (2.10GHz Intel(R) Xeon(R) Gold 6230) machine, using a pure `gpytorch/pytorch/numpy` implementation. All other computations were run on a Xeon Skylake 5218 2.3 GHz GPU with 12 Go of RAM.

# E ADDITIONAL EXPERIMENTS

## E.1 Computation time experiments

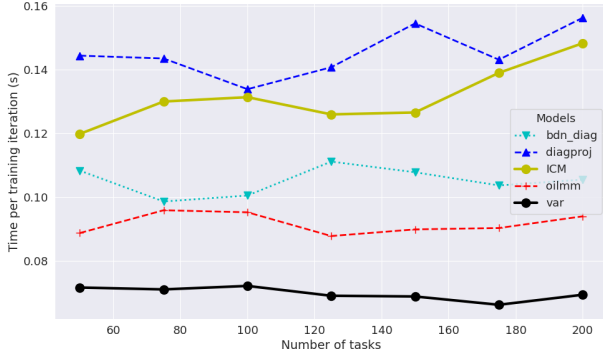
In section 5.2 we displayed training durations for a scaling experiment 4 and mentioned additional observations, which we present here.

We first have to explain the negative relation between  $t_{train}$  and number of latent of tasks  $p$  in some part of figure 4. One simple explanation arises: as specified in Annex D, models are trained until a convergence criterion is met, not in a fixed budget of iterations, so the higher training time could simply be due to a larger number of iterations stemming from a less favorable optimization landscape. To verify that it is correct, we can simply plot the quantity  $t_{train}/N_{iter}$  against  $p$  for the same results: this is done in figure 5a. When doing so, we find the duration of an iteration to be indeed increasing or constant with the number of tasks.

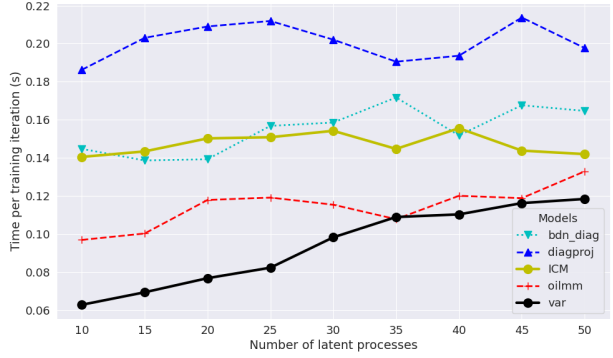
We also stated in section 5.2 that a training time (per iteration) nearly constant in the number of tasks was expected for the variational model and all PLMCs, as the relevant quantity in these cases is rather the number of latent processes  $q$ , which these models scale linearly in. This is made more precise in Annex C, and is verified experimentally in figure 5b: the duration of an iteration indeed scales in a roughly affine manner with  $q$ .

## E.2 Number of tasks and latent processes

We mentioned in section 5.2 differentiated behaviors of the models when either  $p$  or  $q$  was varied while keeping the other fixed. Results for such experiments are displayed in figure 6. The surprising observation is that models `ICM`, `oilmm` and `diagproj` seem most sensitive to the *absolute number of tasks and latent processes*, not to their relative values – it is a common observation that having  $p \simeq q$  in LMC-based models can result in instability for instance. Here, it is rather the absolute complexity of the problem which seems to be at play, and this complexity increases with both  $p$  and  $q$ . For the `ICM` this result is perhaps not surprising, as its kernel structure is unsuited to our synthetic data, which contains as many lengthscales as



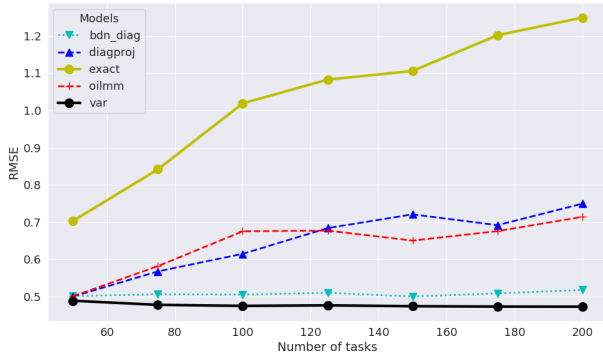
(a) Variable  $p$ , fixed  $q = 25$



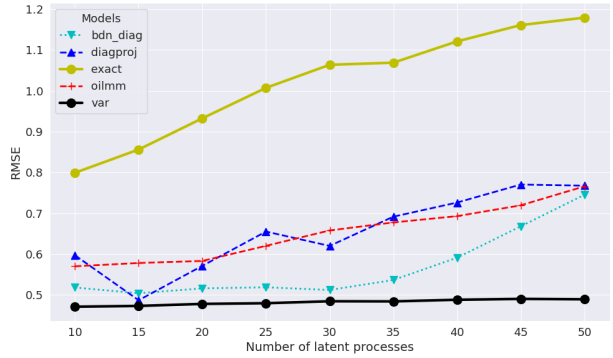
(b) Variable  $q$ , fixed  $p = 100$

Figure 5: Duration of a training iteration for several models, with a) increasing number of tasks and fixed number of latent processes, and b) the opposite. Averaged over  $N_{rep} = 20$  random datasets

there are latent processes<sup>10</sup> (see data description in section 5.2). For PLMCs it may be due to the difficulty of separating noise from data. Figure 2 shows indeed that in this setup noise complexity has a strong impact on the accuracy of all models, so it is perhaps not abnormal that increasing global problem complexity affects disproportionately PLMCs, as their mixing matrix interacts with their noise matrix through the DPN assumption and the presented parametrization. The fact that model `bdn_diag`, equipped with a simpler and more robust noise structure, behave better in this experiment corroborates this hypothesis.



(a) Variable  $p$ , fixed  $q = 25$



(b) Variable  $q$ , fixed  $p = 100$

Figure 6: RMSE of several models, with a) increasing number of tasks and fixed number of latent processes, and b) the opposite. Default noise parameters ( $\mu_{noise} = 0.1$ ,  $\mu_{str} = 0.9$ ,  $q_{noise} = 25$ ). Averaged over  $N_{rep} = 20$  random datasets

<sup>10</sup>Yet the range of these lengthscales is kept constant, whatever  $p$  and  $q$  may be.

### E.3 Bramblemet tidal height dataset

This dataset consists in weather data collected by four weather stations located in Southampton, UK <sup>11</sup>. We focus on the tidal height data amongst all records: we therefore obtain 4 outputs and only one input, time (time-series data). Two weeks of observations (the two first of June 2020) were retained; 3 of the 4 outputs channels were linearly interpolated to match the time frame of the Bramblemet station, taken as reference. We subsampled the data to the quarter of its frequency, for computational ease and to improve convergence. The learning task was to predict a day of measurements, put aside of the training data. In order to correctly modelize this highly periodic data, we selected a spectral mixture kernel (Wilson and Adams [2013]). This task proved to be very challenging for all models, which tended to get stuck in local minima – in particular this of a prediction worth zero everywhere – despite proper initialization of parameters. We therefore tried all combinations of number of latent processes  $q$  and number of spectral components  $N_{mix}$ , in the ranges  $\llbracket 1; p \rrbracket$  and  $\llbracket 2; 5 \rrbracket$  respectively, and selected the best outcome for each model. Results are displayed in table 6, with an illustration in figure 7: we can see that only PLMCs managed to converge to a decent approximation. Once again, we also observe the beneficial impact of the BDN assumption 2 on both training time and accuracy, in particular when coupled with the diagonal  $\mathbf{\hat{B}}$  parametrization in this case. Most importantly, this experience proves that PLMCs can accommodate complex kernels to perform tasks such as time series forecasting.

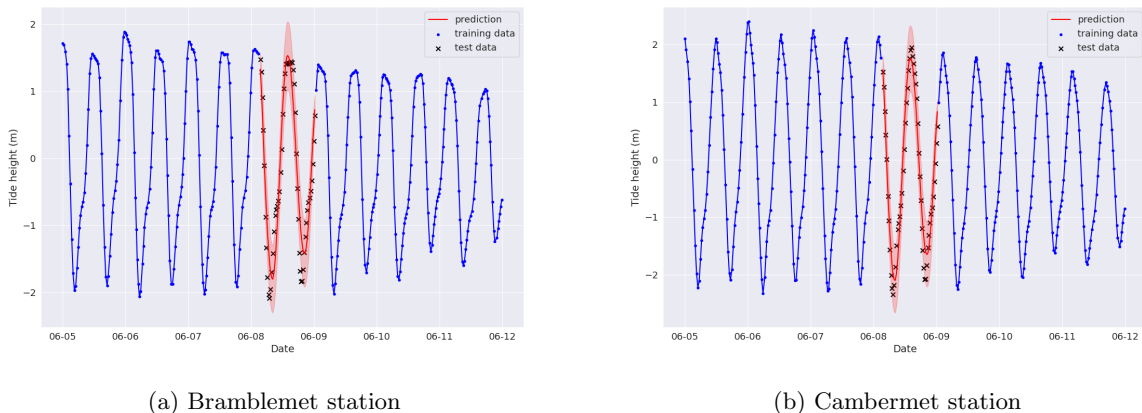


Figure 7: Illustration of predictions of the `bdn_diag` model on the tidal height dataset. ( $q = 1$ ,  $N_{mix} = 5$ )

### E.4 Ship maintenance dataset

This dataset was introduced in Coraddu et al. [2014], and available at the UCI machine learning repository <sup>12</sup>. It consists in numerical simulations of the propulsion system (gas turbine) of a naval vessel (frigate), fine-tuned on real data to be representative of a possible real ship. Inputs of the dataset are ship speed and simulation coefficients reflecting the condition of the engine: compressor degradation coefficient  $kMc$

<sup>11</sup>It's available for instance at <https://github.com/GAMES-UChile/mogptk>, or on the websites of said stations: <http://www.bramblemet.co.uk>, <http://www.cambermet.co.uk>, <http://www.chiemet.co.uk> and <http://www.sotonmet.co.uk>.

<sup>12</sup><http://archive.ics.uci.edu/dataset/316/condition+based+maintenance+of+naval+propulsion+plants>

Table 4: Results of the *Bramblemet* experiment  
( $p = 4, n = 156, d = 1$ )

Model	$N_{iter}$	$t_{train}$	RMSE	PVA	$q$	$N_{mix}$
proj	5003	100	0.375	0.42	1	5
diagproj	4204	305	0.414	0.27	4	5
bdn	5684	501	0.353	0.25	4	5
bdn_diag	4231	75	0.301	-0.04	1	5
oilmm	609	9	1.269	0.24	1	4
ICM	537	31	1.271	0.22	4	5
var	541	13	1.271	0.23	1	2

Table 5: Results of the *Ship maintenance* experiment  
( $p = 12, n = 2287, d = 3, q = 3, N_{ind} = 500$ )

Model	$N_{iter}$	$t_{train}$	RMSE	$Q_{L1}^{95}$	PVA
bdn	6945	542	0.080	0.139	-0.60
diagproj	7019	536	0.081	0.148	-0.86
proj	6719	569	0.082	0.149	-0.70
bdn_diag	7536	586	0.093	0.187	-0.38
oilmm	2021	432	0.194	0.400	2.49
ICM	4516	3427	0.069	0.118	-0.39
var	3129	313	0.075	0.161	-0.52

Table 6: Additional experimental data

and turbine degradation coefficient kMt. These three inputs are sampled on a uniform grid with a good granularity. Outputs are 14 variables describing the operational state of the system: torques, pressures, fuel flow... We discarded two of these outputs presenting zero or near-zero variance, and centered and normalized the other with their normal deviation. For computational convenience, we subsampled the fine input grid by a factor of 5, and stored apart the last 100 points of the dataset for testing, ending up with 2287 training points. We once again used a Matérn-5/2 kernel with input-specific parametrized lengthscales for all models. Independent task noises (diagonal  $\Sigma$ ) were this time used for models var and ICM, yielding better results than fully general multitask gaussian likelihoods. Results are displayed in table 6: once more PLMCs are nearly as accurate as the baselines, more accurate than the OILMM, faster than the ICM, and they sometimes yield better variance estimation (model bdn\_diag has the best PVA in this case).

## F MISSING PROOFS

### F.1 Preliminary considerations

**Notation.** We adopt the following standard notation for any matrix  $\mathbf{M}$ :  $\mathbf{Sym}(\mathbf{M}) = \frac{\mathbf{M} + \mathbf{M}^T}{2}$ .

**Kronecker product manipulation.** We recall elementary properties of the Kronecker product :

$$(\mathbf{A} \otimes \mathbf{B})(\mathbf{C} \otimes \mathbf{D}) = (\mathbf{AC} \otimes \mathbf{BD}) \quad \text{for all matrices } \mathbf{A}, \mathbf{B}, \mathbf{C}, \mathbf{D} \text{ for which the products are defined ;} \quad (11)$$

$$(\mathbf{C}^T \otimes \mathbf{A})\mathbf{vec}(\mathbf{B}) = \mathbf{vec}(\mathbf{ABC}) \quad (12)$$

$$(\mathbf{A} \otimes \mathbf{B})^{-1} = \mathbf{A}^{-1} \otimes \mathbf{B}^{-1} \quad (\text{the inverse exists if and only if } \mathbf{A}^{-1}, \mathbf{B}^{-1} \text{ exist}) \quad (13)$$

**An identity on gaussian processes.**

**Lemma 2.**

$$\mathbb{E}_{U|Y} [\mathbb{E}_{u^*}(\mathbf{u}^* | \mathbf{Y}, \mathbf{U})] = \mathbf{Diag}(\mathbf{k}_{i^*}^T) \mathbf{Diag}(\mathbf{K}_i^{-1}) \mathbb{E}_{U|Y}(\mathbf{U}_v | \mathbf{Y}) \quad (14)$$

*Proof.*

$$\begin{aligned}
\mathbb{E}_{U|Y} [\mathbb{E}_{u^*}(\mathbf{u}^*|\mathbf{Y}, \mathbf{U})] &= \int \mathbb{E}_{u^*}(\mathbf{u}^*|\mathcal{Y}, \mathbf{U}) p(\mathbf{U}|\mathbf{Y}) d\mathbf{U} \\
&= \int \mathbf{Diag}(\mathbf{k}_{i^*}^T) \mathbf{Diag}(\mathbf{K}_i^{-1}) \mathbf{U}_v p(\mathbf{U}|\mathbf{Y}) d\mathbf{U} \\
&= \mathbf{Diag}(\mathbf{k}_{i^*}^T) \mathbf{Diag}(\mathbf{K}_i^{-1}) \mathbb{E}_{U|Y}(\mathbf{U}_v|\mathbf{Y})
\end{aligned}$$

The second equality holds by the conditioning property of GPs, and because  $\mathbb{E}_{u^*}(\mathbf{u}^*|\mathbf{Y}, \mathbf{U})$  doesn't depend on  $\mathbf{Y}$  (conditionally on their corresponding latent values, observed values of a GP are independent of all other variables of the model).  $\square$

**A useful matrix identity.**

**Lemma 3.** *For all invertible matrices  $\mathbf{A}, \mathbf{B}$  and all matrix  $\mathbf{C}$  conformable with them,  $\mathbf{C}^T(\mathbf{C}\mathbf{A}\mathbf{C}^T + \mathbf{B})^{-1}\mathbf{C} = (\mathbf{A} + \mathbf{C}^T\mathbf{B}\mathbf{C})^{-1}$ . Note that  $\mathbf{A}$  and  $\mathbf{B}$  are not necessarily of the same size, so  $\mathbf{C}$  can be rectangular.*

*Proof.*

$$\begin{aligned}
\mathbf{C}^T(\mathbf{C}\mathbf{A}\mathbf{C}^T + \mathbf{B})^{-1}\mathbf{C} &= \mathbf{A}^{-1} (\mathbf{A}\mathbf{C}^T(\mathbf{C}\mathbf{A}\mathbf{C}^T + \mathbf{B})^{-1}\mathbf{C}\mathbf{A}) \mathbf{A}^{-1} \\
&= \mathbf{A}^{-1} (\mathbf{A}\mathbf{C}^T(\mathbf{C}\mathbf{A}\mathbf{C}^T + \mathbf{B})^{-1}\mathbf{C}\mathbf{A} - \mathbf{A}) \mathbf{A}^{-1} + \mathbf{A}^{-1} \\
&= \mathbf{A}^{-1} - (\mathbf{A}^{-1} + \mathbf{C}^T\mathbf{B}\mathbf{C})^{-1} \mathbf{A}^{-1} + \mathbf{A}^{-1} \quad \text{by backward Woodbury's identity} \\
&= (\mathbf{A} + \mathbf{C}^T\mathbf{B}\mathbf{C})^{-1} \quad \text{again by backward Woodbury's identity.}
\end{aligned}$$

$\square$

## F.2 Proofs of the propositions

### Prop 1

*Proof.* All involved variables being jointly gaussian, we know that  $p(\mathbf{U}|\mathbf{Y})$  is gaussian ; it suffices to find its mean and variance. By Baye's rule,  $p(\mathbf{U}|\mathbf{Y}) \propto p(\mathbf{Y}|\mathbf{U})p(\mathbf{U})$ , the proportionality constant being the likelihood  $p(\mathbf{Y})$  which is independant of the latent variables  $\mathbf{U}$ . By definition of the model, we have (using the symmetry of  $\Sigma$  in the second equality):

$$\begin{aligned}
p(\mathbf{Y}|\mathbf{U})p(\mathbf{U}) &\propto \exp\left\{-\frac{1}{2}(\mathbf{Y}_v - (\mathbf{H} \otimes \mathbf{I}_n)\mathbf{U}_v)^T (\Sigma^{-1} \otimes \mathbf{I}_n) (\mathbf{Y}_v - (\mathbf{H} \otimes \mathbf{I}_n)\mathbf{U}_v) - \frac{1}{2}\mathbf{U}_v^T \mathbf{Diag}(\mathbf{K}_i^{-1})\mathbf{U}_v\right\} \\
&\propto \exp\left\{-\frac{1}{2}\mathbf{Y}_v^T (\Sigma^{-1} \otimes \mathbf{I}_n)\mathbf{Y}_v - 2\mathbf{U}_v^T (\mathbf{H}^T \Sigma^{-1} \otimes \mathbf{I}_n)\mathbf{Y}_v + \mathbf{U}_v^T (\mathbf{Diag}(\mathbf{K}_i^{-1}) + \mathbf{H}^T \Sigma^{-1} \mathbf{H} \otimes \mathbf{I}_n)\mathbf{U}_v\right\}
\end{aligned}$$

On the other hand,  $p(\mathbf{Y}|\mathbf{U})p(\mathbf{U})$  being gaussian, there exists a covariance matrix  $\tilde{\mathbf{K}}$  and a mean vector  $\hat{\mathbf{U}}_v$  such that :

$$\begin{aligned}
p(\mathbf{Y}|\mathbf{U})p(\mathbf{U}) &\propto \exp\left\{-\frac{1}{2}(\mathbf{U}_v - \hat{\mathbf{U}}_v)^T \tilde{\mathbf{K}}^{-1}(\mathbf{U}_v - \hat{\mathbf{U}}_v)\right\} \\
&= \exp\left\{-\frac{1}{2}\mathbf{U}_v^T \tilde{\mathbf{K}}^{-1}\mathbf{U}_v - 2\mathbf{U}_v^T \tilde{\mathbf{K}}^{-1}\hat{\mathbf{U}}_v + \hat{\mathbf{U}}_v^T \tilde{\mathbf{K}}^{-1}\hat{\mathbf{U}}_v\right\}
\end{aligned}$$

Therefore, to compute  $\tilde{\mathbf{K}}$  and  $\hat{\mathbf{U}}$ , one simply has to identify the terms in  $\mathbf{U}$  between the above expressions, as all the terms which don't depend on  $\mathbf{U}$  are compensated by the likelihood (denominator of Baye's formula). Proceeding as such, we obtain :

$$\begin{cases} \tilde{\mathbf{K}}^{-1} &= \text{Diag}(\mathbf{K}_i^{-1}) + \mathbf{H}^T \boldsymbol{\Sigma}^{-1} \mathbf{H} \otimes \mathbf{I}_n \\ \tilde{\mathbf{K}}^{-1} \hat{\mathbf{U}}_v &= (\mathbf{H}^T \boldsymbol{\Sigma}^{-1} \otimes \mathbf{I}_n) \mathbf{Y}_v = \text{vec}(\mathbf{Y}^T \boldsymbol{\Sigma}^{-1} \mathbf{H}) \end{cases}$$

By definition,  $\hat{\mathbf{U}}_v$  is the mean vector of  $p(\mathbf{U}_v | \mathbf{Y})$  and  $\tilde{\mathbf{K}}$  is its covariance matrix, hence the result.  $\square$

## Prop 2

*Proof.* We start with the estimated variance. By hypothesis of the model, the  $u_i$ 's follow GPs of kernels  $k_i$ 's, so we have by lemma 2:

$$\begin{aligned} \mathbb{E}(\hat{\mathbf{u}}_* | \mathbf{Y}) &= \text{Diag}(\mathbf{k}_{i_*}^T) \text{Diag}(\mathbf{K}_i^{-1}) \mathbb{E}(\mathbf{U}_v | \mathbf{Y}) \\ &= \text{Diag}(\mathbf{k}_{i_*}^T) \text{Diag}(\mathbf{K}_i^{-1}) [\text{Diag}(\mathbf{K}_i^{-1}) + \mathbf{H}^T \boldsymbol{\Sigma}^{-1} \mathbf{H} \otimes \mathbf{I}_n]^{-1} (\mathbf{H}^T \boldsymbol{\Sigma}^{-1} \otimes \mathbf{I}_n) \mathbf{Y}_v \\ &= \text{Diag}(\mathbf{k}_{i_*}^T) [\text{Diag}(\mathbf{K}_i) + (\mathbf{H}^T \boldsymbol{\Sigma}^{-1} \mathbf{H})^{-1} \otimes \mathbf{I}_n]^{-1} ((\mathbf{H}^T \boldsymbol{\Sigma}^{-1} \mathbf{H})^{-1} \otimes \mathbf{I}_n) (\mathbf{H}^T \boldsymbol{\Sigma}^{-1} \otimes \mathbf{I}_n) \mathbf{Y}_v \\ &= \text{Diag}(\mathbf{k}_{i_*}^T) [\text{Diag}(\mathbf{K}_i) + (\mathbf{H}^T \boldsymbol{\Sigma}^{-1} \mathbf{H})^{-1} \otimes \mathbf{I}_n]^{-1} \text{vec}(\mathbf{Y}^T \boldsymbol{\Sigma}^{-1} \mathbf{H} (\mathbf{H}^T \boldsymbol{\Sigma}^{-1} \mathbf{H})^{-1}) \end{aligned}$$

where the second equality is from prop.3, the third one from the matrix equality  $\mathbf{A}^{-1}(\mathbf{A}^{-1} + \mathbf{B}^{-1})^{-1} = (\mathbf{A} + \mathbf{B})^{-1} \mathbf{B}$  and the fourth one from basic facts 11 and 12.

We now compute the estimated variance from the law of total variance, conditioning on  $\mathbf{U}$ :  $\mathbb{V}(\hat{\mathbf{u}}_* | \mathbf{Y}) = \mathbb{E}_{U|Y} [\mathbb{V}(\hat{\mathbf{u}}_* | \mathbf{Y}, \mathbf{U})] + \mathbb{V}_{U|Y} [\mathbb{E}(\hat{\mathbf{u}}_* | \mathbf{Y}, \mathbf{U})]$ , where the subscript  $U|Y$  means that  $\mathbb{E}_{U|Y}(f(\mathbf{U})) = \int f(\mathbf{U}) p(\mathbf{U} | \mathbf{Y}) d\mathbf{U}$ . From there, we omit this subscript and treat each term separately. We also recall that  $p(\mathbf{u}^* | \mathbf{Y}, \mathbf{U})$  doesn't depend on  $\mathbf{Y}$  (conditionnally on their corresponding latent values, observed values of a GP are independent on all other variables of the model, and therefore  $\mathbb{E}_{u^*}(\mathbf{u}^* | \mathbf{Y}, \mathbf{U})$  doesn't depend on  $\mathbf{Y}$  (idem for the variance). It comes :

$$\begin{aligned} \mathbb{E}[\mathbb{V}(\hat{\mathbf{u}}_* | \mathbf{Y}, \mathbf{U})] &= \mathbb{E}[\text{Diag}(k_{i_{**}}) - \text{Diag}(\mathbf{k}_{i_*}^T) \text{Diag}(\mathbf{K}_i^{-1}) \text{Diag}(\mathbf{k}_{i_*})] \\ &= (\text{Diag}(k_{i_{**}}) - \text{Diag}(\mathbf{k}_{i_*}^T) \text{Diag}(\mathbf{K}_i^{-1}) \text{Diag}(\mathbf{k}_{i_*})) \end{aligned}$$

where the second equality holds because the term inside the expectation is deterministic. For the second term, we have :

$$\begin{aligned} \mathbb{V}_{U|Y} [\mathbb{E}(\hat{\mathbf{u}}_* | \mathbf{Y}, \mathbf{U})] &= \mathbb{E}_{U|Y} [\mathbb{E}((\hat{\mathbf{u}}_* | \mathbf{Y}, \mathbf{U})^2)] - \mathbb{E}_{U|Y} [\mathbb{E}(\hat{\mathbf{u}}_* | \mathbf{Y}, \mathbf{U})]^2 \\ &= \text{Diag}(\mathbf{k}_{i_*}^T) \text{Diag}(\mathbf{K}_i^{-1}) \mathbb{E}(\mathbf{U}_v^2 | \mathbf{Y}) \text{Diag}(\mathbf{K}_i^{-1}) \text{Diag}(\mathbf{k}_{i_*}) - \text{Diag}(\mathbf{k}_{i_*}^T) \text{Diag}(\mathbf{K}_i^{-1}) \mathbb{E}(\mathbf{U}_v | \mathbf{Y})^2 \text{Diag}(\mathbf{K}_i^{-1}) \text{Diag}(\mathbf{k}_{i_*}) \\ &= \text{Diag}(\mathbf{k}_{i_*}^T) \text{Diag}(\mathbf{K}_i^{-1}) \mathbb{V}(\mathbf{U}_v | \mathbf{Y}) \text{Diag}(\mathbf{K}_i^{-1}) \text{Diag}(\mathbf{k}_{i_*}) \\ &= \text{Diag}(\mathbf{k}_{i_*}^T) \text{Diag}(\mathbf{K}_i^{-1}) [\text{Diag}(\mathbf{K}_i^{-1}) + \mathbf{H}^T \boldsymbol{\Sigma}^{-1} \mathbf{H} \otimes \mathbf{I}_n]^{-1} \text{Diag}(\mathbf{K}_i^{-1}) \text{Diag}(\mathbf{k}_{i_*}) \end{aligned}$$

where the second equality stems from a relation analog to this of lemma 2, and the fourth is from prop.3.

Combining the two terms, it comes :  $\mathbb{V}(\hat{\mathbf{u}}_*|\mathbf{Y})$

$$\begin{aligned} &= \text{Diag}(k_{i^{**}}) - \text{Diag}(\mathbf{k}_{i^*}^T) \left[ \text{Diag}(\mathbf{K}_i^{-1}) - \text{Diag}(\mathbf{K}_i^{-1}) (\text{Diag}(\mathbf{K}_i^{-1}) + \mathbf{H}^T \boldsymbol{\Sigma}^{-1} \mathbf{H} \otimes \mathbf{I}_n)^{-1} \text{Diag}(\mathbf{K}_i^{-1}) \right] \text{Diag}(\mathbf{k}_{i^*}) \\ &= \text{Diag}(k_{i^{**}}) - \text{Diag}(\mathbf{k}_{i^*}^T) \left[ \text{Diag}(\mathbf{K}_i) + (\mathbf{H}^T \boldsymbol{\Sigma}^{-1} \mathbf{H})^{-1} \otimes \mathbf{I}_n \right]^{-1} \text{Diag}(\mathbf{k}_{i^*}) \end{aligned}$$

where the second equality is from the Woodburry-type identity  $\mathbf{A}^{-1} - \mathbf{A}^{-1}(\mathbf{A}^{-1} + \mathbf{B}^{-1})^{-1}\mathbf{A}^{-1} = (\mathbf{A} + \mathbf{B})^{-1}$ .  $\square$

**Prop 3 to 5** Propositions 3 and 5 are proven in annexes D, E and F of Bruinsma et al. [2020]. We add a few supplementary clarifications:

- Proof of ( $\mathbf{TY}$  sufficient statistic for  $\mathbf{U}$ )  $\Rightarrow (p(\mathbf{U}|\mathbf{Y}) = p(\mathbf{U}|\mathbf{TY}))$ :

$$\begin{aligned} p(\mathbf{U}|\mathbf{Y}) &= \frac{p(\mathbf{U}, \mathbf{Y})}{p(\mathbf{Y})} = \frac{p(\mathbf{U}, \mathbf{Y}, \mathbf{TY})}{p(\mathbf{Y})} = \frac{p(\mathbf{Y}|\mathbf{TY}, \mathcal{U})p(\mathbf{TY}, \mathbf{U})}{p(\mathbf{Y})} = \frac{p(\mathbf{Y}|\mathbf{TY})p(\mathbf{TY}, \mathbf{U})}{p(\mathbf{Y})} \\ &= \frac{p(\mathbf{Y}, \mathbf{TY})p(\mathbf{TY}, \mathbf{U})}{p(\mathbf{TY})p(\mathbf{Y})} = p(\mathbf{TY}|\mathbf{Y}) \frac{p(\mathbf{TY}, \mathbf{U})}{p(\mathbf{TY})} = 1 \times p(\mathbf{U}|\mathbf{TY}) \end{aligned} \quad (15)$$

where the fourth equality is precisely the definition of  $\mathbf{TY}$  being a sufficient statistic of  $\mathbf{U}$  for the data  $\mathbf{Y}$  : conditionally on  $\mathbf{TY}$ , the probability of the data doesn't depend on  $\mathbf{U}$ .

- Proof of  $\mathbf{TY}|\mathbf{U} \sim \mathcal{N}(\mathbf{U}_v, \boldsymbol{\Sigma}_P \otimes \mathbf{I}_n)$  : by definition of the LMC  $\mathbf{Y}_v|\mathbf{U} \sim \mathcal{N}((\mathbf{H} \otimes \mathbf{I}_n)\mathbf{U}_v, \boldsymbol{\Sigma} \otimes \mathbf{I}_n)$ , so  $p(\mathbf{TY}|\mathbf{U}) = p((\mathbf{T} \otimes \mathbf{I}_n)\mathbf{Y}_v|\mathbf{U}) = \mathcal{N}((\mathbf{T} \otimes \mathbf{I}_n)(\mathbf{H} \otimes \mathbf{I}_n)\mathbf{U}_v, \mathbf{T}\boldsymbol{\Sigma}\mathbf{T}^T \otimes \mathbf{I}_n) = \mathcal{N}(\mathbf{U}_v, \boldsymbol{\Sigma}_P \otimes \mathbf{I}_n)$  because  $\mathbf{TH} = \mathbf{I}_q$ .

Proof of prop.4 is essentially trivial, all involved matrices being block-diagonal if the DPN condition stands (in particular,  $\mathcal{K} = \text{Diag}(\mathbf{K}_i) + \boldsymbol{\Sigma}_P \otimes \mathbf{I}_n = \text{Diag}(\mathbf{K}_i + \sigma_i^2 \mathbf{I}_n)$ ). Notice that for any block-diagonal matrix  $\tilde{\mathbf{D}} = \text{Diag}(\mathbf{D}_i)$  and any matrix  $\mathbf{M}$  such that the blocksize of  $\tilde{\mathbf{D}}$  matches the column size of  $\mathbf{M}$ , we have  $\tilde{\mathbf{D}} \text{vec}(\mathbf{M}) = \text{Diag}(\mathbf{D}_i \mathbf{M}_i)$ , where  $\mathbf{M}_i$  is the  $i$ -th column of  $\mathbf{M}$ ; this explains the  $\mathbf{T}_i$ 's present in the final expression.

### Lemma 1

*Proof.* It suffices to write that  $\mathcal{S} = (\mathbf{Q}\mathbf{Q}^T + \mathbf{Q}_\perp\mathbf{Q}_\perp^T) \mathcal{S} (\mathbf{Q}\mathbf{Q}^T + \mathbf{Q}_\perp\mathbf{Q}_\perp^T)$  (because  $\mathbf{Q}\mathbf{Q}^T$  and  $\mathbf{Q}_\perp\mathbf{Q}_\perp^T$  are supplementary orthogonal projectors), and then set  $\mathbf{A} = \mathbf{Q}^T \mathcal{S} \mathbf{Q}$ ,  $\mathbf{B} = \mathbf{Q}_\perp^T \mathcal{S} \mathbf{Q}_\perp$ ,  $\mathbf{C} = \mathbf{Q}^T \mathcal{S} \mathbf{Q}_\perp$ . Another way of seeing this is by noticing that  $\mathbf{A}$ ,  $\mathbf{B}$ ,  $\mathbf{C}$  and  $\mathbf{C}^T$  are the blocks of the representation of  $\mathcal{S}$  in the basis spanned by  $\mathbf{Q}$  and  $\mathbf{Q}_\perp$ .  $\square$

### Prop 6

*Proof.* We have  $\mathbf{H}^T \boldsymbol{\Sigma}^{-1} \mathbf{H} = \mathbf{R}^T \mathbf{Q}^T \boldsymbol{\Sigma}^{-1} \mathbf{Q} \mathbf{R}$ ; moreover,  $\mathbf{Q}^T \mathbf{Q}_\perp = \mathbf{0}$ ,  $\mathbf{Q}_\perp^T \mathbf{Q} = \mathbf{0}$  and  $\mathbf{Q}^T \mathbf{Q} = \mathbf{I}_q$  because the columns of  $\mathbf{Q}$  and  $\mathbf{Q}_\perp$  are mutually orthonormal. Thus we see that the only term from the decomposition of  $\boldsymbol{\Sigma}^{-1}$  that is preserved by left- and right-multiplication by  $\mathbf{Q}$  and  $\mathbf{Q}^T$  is  $\mathbf{A}$  :  $\mathbf{H}^T \boldsymbol{\Sigma}^{-1} \mathbf{H} = \mathbf{R}^T \mathbf{A} \mathbf{R} \Leftrightarrow \boldsymbol{\Sigma}_P = \mathbf{R}^{-1} \mathbf{A}^{-1} \mathbf{R}^{-T}$ . Moreover,  $(\mathbf{H}^T \boldsymbol{\Sigma}^{-1} \mathbf{H} \text{ is diagonal}) \Leftrightarrow (\mathbf{R}^T \mathbf{A} \mathbf{R} = \mathbf{D} \text{ for some diagonal matrix } \mathbf{D}) \Leftrightarrow (\mathbf{A} = \mathbf{R}^{-T} \mathbf{D} \mathbf{R}^{-1} \text{ for some diagonal matrix } \mathbf{D})$ .  $\square$



**Prop 7**

*Proof.* The proof is by direct calculation. Starting from the suggested factorized form, one easily arrives at :

$\mathbf{Q}_+ \mathbf{R}_+^{-\mathbf{T}} \mathbf{D}_+^{-1} \mathbf{R}_+^{-1} \mathbf{Q}_+^{\mathbf{T}} = \mathbf{Q} \mathbf{R}^{-\mathbf{T}} \mathbf{D} \mathbf{R}^{-1} \mathbf{Q}^{\mathbf{T}} + \mathbf{Q}_\perp \mathbf{B} \mathbf{Q}_\perp^{\mathbf{T}} + 2 \mathbf{Sym}(\mathbf{Q} \mathbf{R}^{-\mathbf{T}} \mathbf{M} \mathbf{Q}_\perp^{\mathbf{T}})$ . From this, we can identify terms with the above additive decomposition (where every identification is valid), which yields the announced formulas for  $\mathbf{D}$  and  $\mathbf{M}$ . □

**Prop 8**

*Proof.* First notice that  $\tilde{\mathbf{B}}$  is the Schur complement of  $\Sigma_{\mathbf{P}}$  inside  $\mathbf{D}_+$ . It happens that providing a pair of Schur complements of a symmetric matrix and any diagonal block of itself or its inverse fully specifies this matrix. Indeed, using the previous tilded notations for the blocks of  $\Sigma$ , blockwise matrix inversion formulas show that  $\tilde{\mathbf{D}} = \Sigma_{\mathbf{P}} + \Sigma_{\mathbf{P}} \tilde{\mathbf{M}} \tilde{\mathbf{B}} \mathbf{M}^{\mathbf{T}} \Sigma_{\mathbf{P}}$ ,  $\tilde{\mathbf{M}} = -\Sigma_{\mathbf{P}} \tilde{\mathbf{M}} \tilde{\mathbf{B}}$ , and finally  $\mathbf{B} = \tilde{\mathbf{B}}^{-1} + \tilde{\mathbf{B}}^{-1} \tilde{\mathbf{M}}^{\mathbf{T}} \Sigma_{\mathbf{P}}^{-1} \tilde{\mathbf{M}} \tilde{\mathbf{B}}^{-1}$ , so that by the last equality  $\mathbf{B} = \tilde{\mathbf{B}}^{-1} + \mathbf{M}^{\mathbf{T}} \Sigma_{\mathbf{P}} \mathbf{M}$ . Thus we see that all blocks of  $\Sigma^{-1}$  and  $\Sigma$  are expressed from  $\tilde{\mathbf{B}}$ ,  $\Sigma_{\mathbf{P}}$  and  $\mathbf{M}$  without any circular definitions. Moreover, by a standard result,  $\Sigma$  is p.s.d iff its two Schur complements  $\tilde{\mathbf{B}}$  and  $\Sigma_{\mathbf{P}}$  are; see for instance Boyd and Vandenberghe [2004]. □

**Prop 9**

*Proof.* We recall from prop.6 that  $\Sigma_{\mathbf{P}} = \mathbf{D}^{-1}$ . Applying  $\mathbf{H}^{\mathbf{T}}$  to the additive decomposition of  $\Sigma^{-1}$  strikes out the terms beginning with  $\mathbf{Q}_\perp$ , so :

$$\begin{aligned} \mathbf{T} &= \Sigma_{\mathbf{P}} \mathbf{H}^{\mathbf{T}} \Sigma^{-1} = \Sigma_{\mathbf{P}} \mathbf{R}^{\mathbf{T}} \mathbf{Q}^{\mathbf{T}} (\mathbf{Q} \mathbf{A} \mathbf{Q}^{\mathbf{T}} + \mathbf{Q}_\perp \mathbf{B} \mathbf{Q}_\perp^{\mathbf{T}} + \mathbf{Q} \mathbf{C} \mathbf{Q}_\perp^{\mathbf{T}} + \mathbf{Q}_\perp \mathbf{C}^{\mathbf{T}} \mathbf{Q}^{\mathbf{T}}) = \Sigma_{\mathbf{P}} \mathbf{R}^{\mathbf{T}} \mathbf{A} \mathbf{Q}^{\mathbf{T}} + \Sigma_{\mathbf{P}} \mathbf{R}^{\mathbf{T}} \mathbf{C} \mathbf{Q}_\perp^{\mathbf{T}} \\ &= \Sigma_{\mathbf{P}} \mathbf{R}^{\mathbf{T}} \mathbf{A} \mathbf{Q}^{\mathbf{T}} + \Sigma_{\mathbf{P}} \mathbf{M} \mathbf{Q}_\perp^{\mathbf{T}} \quad \text{by definition of } \mathbf{M}. \end{aligned}$$

The first term is equal to  $\Sigma_{\mathbf{P}} \mathbf{R}^{\mathbf{T}} (\mathbf{R}^{-\mathbf{T}} \mathbf{D} \mathbf{R}^{-1}) \mathbf{Q}^{\mathbf{T}} = \mathbf{D}^{-1} \mathbf{D} \mathbf{R}^{-1} \mathbf{Q}^{\mathbf{T}} = \mathbf{H}^+$  (the latter equality being a standard result about the Moore-Penrose pseudoinverse). We can reformulate the second one to show that it is invariant to the choice of  $\mathbf{Q}_\perp$  : starting from its previous expression, we have  $\Sigma_{\mathbf{P}} \mathbf{H}^{\mathbf{T}} \mathbf{Q} \mathbf{C} \mathbf{Q}_\perp^{\mathbf{T}} = \Sigma_{\mathbf{P}} \mathbf{H}^{\mathbf{T}} \mathbf{Q} (\mathbf{Q}^{\mathbf{T}} \Sigma^{-1} \mathbf{Q}_\perp) \mathbf{Q}_\perp^{\mathbf{T}} = \Sigma_{\mathbf{P}} \mathbf{H}^{\mathbf{T}} \mathbf{P} \Sigma^{-1} \mathbf{P}_\perp^{\mathbf{T}}$ , with  $\mathbf{P}$  the orthogonal projector onto  $Span(\mathbf{Q})$  and  $\mathbf{P}_\perp$  the orthogonal projector onto  $Span(\mathbf{Q}_\perp) = Span(\mathbf{Q})^\perp$ . The claim is thus clearly proven:  $\mathbf{Q}_\perp \mathbf{Q}_\perp^{\mathbf{T}}$  is only one possible expression of the orthogonal projector on  $Span(\mathbf{Q})^\perp$ , any other orthogonal supplement of  $\mathbf{Q}$  would yield the same result. □

**Prop. 10**

*Proof.* We start from an intermediary expression taken from the appendix G of Bruinsma et al. [2020] under the DPN hypothesis :

$$-2 \log p(\mathbf{Y}) = (p-q)n \log 2\pi + n \log \frac{|\Sigma|}{|\Sigma_{\mathbf{P}}|} + \sum_{j=1}^n \mathbf{Y}_j (\Sigma^{-1} - \mathbf{T}^{\mathbf{T}} \Sigma_{\mathbf{P}}^{-1} \mathbf{T}) \mathbf{Y}_j^{\mathbf{T}} + \sum_{i=1}^q \log \mathcal{N}(\mathbf{Y} \mathbf{T}_i | \mathbf{0}, \mathbf{K}_i + \sigma_i \mathbf{I}_n) \quad (16)$$

where the second term represents the noise lost by projection, the third is the data lost by projection and the last is the standard GP MLL of the independent latent processes. Plugging in the factorization of prop.7, we just reformulate the second and third terms on the right-hand side. Let's start with the second,

corresponding to the discarded noise : using the quantities from the previous section, it suffices to note that with the suggested factorization  $|\Sigma| = |\mathbf{R}|^2 |\mathbf{D}_+|$ . Then, by Schur's determinant formula (determinant of a four-blocks matrix),  $|\mathbf{D}_+| = |\tilde{\mathbf{B}}| |\tilde{\mathbf{D}} - \tilde{\mathbf{M}} \tilde{\mathbf{B}}^{-1} \tilde{\mathbf{M}}^T| = |\tilde{\mathbf{B}}| |\Sigma_{\mathbf{P}}|$ . We now address the third term. The proof of (9) shows that  $\mathbf{H}^T \Sigma^{-1} = \Sigma_{\mathbf{P}}^{-1} \mathbf{T} = \Sigma_{\mathbf{P}}^{-1} \mathbf{R}^{-1} \mathbf{Q}^T + \mathbf{M} \mathbf{Q}_{\perp}^T$ , so :

$$\begin{aligned}
\Sigma^{-1} - \mathbf{T}^T \Sigma_{\mathbf{P}}^{-1} \mathbf{T} &= \Sigma^{-1} - \Sigma^{-1} \mathbf{H} \Sigma_{\mathbf{P}} \mathbf{H}^T \Sigma^{-1} \\
&= \Sigma^{-1} - (\mathbf{Q} \mathbf{R}^{-T} \Sigma_{\mathbf{P}}^{-1} + \mathbf{Q}_{\perp} \mathbf{M}^T) \Sigma_{\mathbf{P}} (\Sigma_{\mathbf{P}}^{-1} \mathbf{R}^{-1} \mathbf{Q}^T + \mathbf{M} \mathbf{Q}_{\perp}^T) \\
&= \Sigma^{-1} - \mathbf{Q}_+ \left( \begin{array}{c|c} \mathbf{R}^{-T} \Sigma_{\mathbf{P}}^{-1} \Sigma_{\mathbf{P}} \Sigma_{\mathbf{P}}^{-1} \mathbf{R}^{-1} & \mathbf{R}^{-T} \Sigma_{\mathbf{P}}^{-1} \Sigma_{\mathbf{P}} \mathbf{M} \\ \hline \mathbf{M}^T \Sigma_{\mathbf{P}} \Sigma_{\mathbf{P}}^{-1} \mathbf{R}^{-1} & \mathbf{M}^T \Sigma_{\mathbf{P}} \mathbf{M} \end{array} \right) \mathbf{Q}_+^T \\
&= \mathbf{Q}_+ \mathbf{R}_+^{-T} \left( \begin{array}{c|c} \Sigma_{\mathbf{P}}^{-1} & \mathbf{M} \\ \hline \mathbf{M}^T & \mathbf{B} \end{array} \right) \mathbf{R}_+^{-1} \mathbf{Q}_+^T - \mathbf{Q}_+ \mathbf{R}_+^{-T} \left( \begin{array}{c|c} \Sigma_{\mathbf{P}}^{-1} & \mathbf{M} \\ \hline \mathbf{M}^T & \mathbf{M}^T \Sigma_{\mathbf{P}} \mathbf{M} \end{array} \right) \mathbf{R}_+^{-1} \mathbf{Q}_+^T \\
&= \mathbf{Q}_{\perp} (\mathbf{B} - \mathbf{M}^T \Sigma_{\mathbf{P}} \mathbf{M}) \mathbf{Q}_{\perp}^T \\
&= \mathbf{Q}_{\perp} \tilde{\mathbf{B}}^{-1} \mathbf{Q}_{\perp}^T \quad \text{by blockwise inversion formula.}
\end{aligned}$$

To see that the obtained expression doesn't depend on a particular choice of  $\mathbf{Q}_{\perp}$ , we just have to prove it for  $\mathbf{Q}_{\perp} \tilde{\mathbf{B}}^{-1} \mathbf{Q}_{\perp}^T$ , as we have already shown it for  $\mathbf{T}$  in prop. 9. Let's write that  $\tilde{\mathbf{B}} = \mathbf{Q}_{\perp}^T \Sigma \mathbf{Q}_{\perp}$  (see corollary 1). Recall that any orthonormal complement of  $\mathbf{Q}$  denoted as  $\mathbf{Q}'$  can be written  $\mathbf{Q}' = \mathbf{Q}_{\perp} \mathbf{W}$  for some square orthonormal matrix  $\mathbf{W}$ . Then:  $\mathbf{Q}' (\mathbf{Q}'^T \Sigma \mathbf{Q}')^{-1} \mathbf{Q}'^T = \mathbf{Q}_{\perp} \mathbf{W} (\mathbf{W}^T \mathbf{Q}_{\perp}^T \Sigma \mathbf{Q}_{\perp} \mathbf{W})^{-1} \mathbf{W} \mathbf{W}^T \mathbf{Q}_{\perp}^T = \mathbf{Q}_{\perp} \mathbf{W} \mathbf{W}^T (\mathbf{Q}_{\perp}^T \Sigma \mathbf{Q}_{\perp})^{-1} \mathbf{W} \mathbf{W}^T \mathbf{Q}_{\perp}^T = \mathbf{Q}_{\perp} (\mathbf{Q}_{\perp}^T \Sigma \mathbf{Q}_{\perp})^{-1} \mathbf{Q}_{\perp}^T$ .  $\square$

### Prop 11

*Proof.* Prop.2 shows that the estimated mean and variance depend on  $\Sigma$  through  $\mathbf{T}$  and  $\Sigma_{\mathbf{P}}$  only. Prop.8 states that  $(\tilde{\mathbf{B}}, \Sigma_{\mathbf{P}}, \mathbf{M})$  is a complete and independent parametrization of  $\Sigma$ , so  $\mathbf{T} = \mathbf{R}^{-1} \mathbf{Q}^T + \Sigma_{\mathbf{P}} \mathbf{M} \mathbf{Q}_{\perp}^T$  (see prop.9) doesn't depend on  $\tilde{\mathbf{B}}$  and neither do the posteriors.

For the second affirmation, notice that the likelihood is invariant under the transformation  $\tilde{\mathbf{B}}^{-1} \leftarrow \mathbf{W} \tilde{\mathbf{B}}^{-1} \mathbf{W}^T$ ,  $\mathbf{Q}_{\perp} \leftarrow \mathbf{Q}_{\perp} \mathbf{W}^T$  with  $\mathbf{W}$  orthonormal, as in particular it doesn't affect  $\mathbf{T}$  (which by prop.9 only depends on  $\text{Im}(\mathbf{Q}_{\perp})$  and not a specific vector basis) ; moreover, such a transformation of  $\mathbf{Q}_{\perp}$  doesn't affect posteriors of the model either, as it only appears in  $\mathbf{T}$  in their expression. Therefore, we can always select the matrix  $\mathbf{W}$  which diagonalizes  $\tilde{\mathbf{B}}^{-1}$ , i.e we can jointly optimize  $\tilde{\mathbf{B}}$  and  $\mathbf{Q}_{\perp}$  while enforcing the diagonality of  $\tilde{\mathbf{B}}$ .  $\square$

### F.3 Matricial proof of prop.2

*We here give another proof of prop.2, which starts from the naive expression of LMC posteriors and uses only matrix algebra. It is a good example of involved manipulations of Kronecker products.*

*Proof.* We start with the "naive" expression of the LMC estimators, as stated in section 1:

$$\mathbb{E}(\hat{\mathbf{y}}_* | \mathbf{Y}) = \mathbf{k}_*^T \mathcal{K}^{-1} \mathbf{Y}_v \quad (17)$$

$$\mathbb{V}(\hat{\mathbf{y}}_* | \mathbf{Y}) = \mathbf{k}_{**} - \mathbf{k}_*^T \mathcal{K}^{-1} \mathbf{k}_* \quad (18)$$

where the kernel considered here is the matricial kernel of the vector-valued GP:  $\mathbf{k}(\mathbf{x}, \mathbf{x}') = \sum_{i=1}^q \mathbf{B}_i k_i(\mathbf{x}, \mathbf{x}')$ , and we recall that  $\mathbf{K} = (\mathbf{H} \otimes \mathbf{I}_n) \mathbf{Diag}(\mathbf{K}_i) (\mathbf{H}^T \otimes \mathbf{I}_n)^{13}$ . Similarly, we have  $\mathbf{k}_* = (\mathbf{H} \otimes \mathbf{I}_n) \mathbf{Diag}(\mathbf{k}_i) \mathbf{H}^T$ , and  $\mathbf{k}_{**} = \mathbf{H} \mathbf{Diag}(\mathbf{k}_{i**}) \mathbf{H}^T$ . Anticipating on the cumbersome writing of Kronecker products, we adopt the following convention : for any matrix  $\mathbf{M}$ ,  $\tilde{\mathbf{M}} \equiv \mathbf{M} \otimes \mathbf{I}_n$ . The properties of the Kronecker product (fact (11)) ensures us that  $\forall \mathbf{M}, \mathbf{N}$ ,  $\tilde{\mathbf{M}}\tilde{\mathbf{N}} = \widetilde{\mathbf{MN}}$ . We start with the expected mean :

$$\begin{aligned}
\mathbf{k}_*^T \mathcal{K}^{-1} \mathbf{Y}_v &= \mathbf{H} \mathbf{Diag}(\mathbf{k}_i^T) \tilde{\mathbf{H}}^T \left[ \tilde{\mathbf{H}} \mathbf{Diag}(\mathbf{K}_i) \tilde{\mathbf{H}}^T + \tilde{\Sigma} \right]^{-1} \mathbf{Y}_v \\
&= \mathbf{H} \mathbf{Diag}(\mathbf{k}_i^T) \tilde{\mathbf{H}}^T \left[ \tilde{\Sigma}^{-1} - \tilde{\Sigma}^{-1} \tilde{\mathbf{H}} \left( \mathbf{Diag}(\mathbf{K}_i^{-1}) + \tilde{\mathbf{H}}^T \tilde{\Sigma}^{-1} \tilde{\mathbf{H}} \right)^{-1} \tilde{\mathbf{H}}^T \tilde{\Sigma}^{-1} \right] \mathbf{Y}_v \\
&= \mathbf{H} \mathbf{Diag}(\mathbf{k}_i^T) \left[ \tilde{\mathbf{H}}^T \tilde{\Sigma}^{-1} - \tilde{\mathbf{H}}^T \tilde{\Sigma}^{-1} \tilde{\mathbf{H}} \left( \mathbf{Diag}(\mathbf{K}_i^{-1}) + \tilde{\Sigma}_P^{-1} \right)^{-1} \tilde{\mathbf{H}}^T \tilde{\Sigma}^{-1} \right] \mathbf{Y}_v \\
&= \mathbf{H} \mathbf{Diag}(\mathbf{k}_i^T) \left[ \tilde{\mathbf{I}}_q - \tilde{\Sigma}_P^{-1} \left( \mathbf{Diag}(\mathbf{K}_i^{-1}) + \tilde{\Sigma}_P^{-1} \right)^{-1} \right] \tilde{\mathbf{H}}^T \tilde{\Sigma}^{-1} \mathbf{Y}_v \\
&= \mathbf{H} \mathbf{Diag}(\mathbf{k}_i^T) \left[ \tilde{\Sigma}_P^{-1} - \tilde{\Sigma}_P^{-1} \left[ \mathbf{Diag}(\mathbf{K}_i^{-1}) + \tilde{\Sigma}_P^{-1} \right]^{-1} \tilde{\Sigma}_P^{-1} \right] \tilde{\Sigma}_P \tilde{\mathbf{H}}^T \tilde{\Sigma}^{-1} \mathbf{Y}_v \\
&= \mathbf{H} \mathbf{Diag}(\mathbf{k}_i^T) \left[ \mathbf{Diag}(\mathbf{K}_i) + \tilde{\Sigma}_P \right]^{-1} \tilde{\Sigma}_P \tilde{\mathbf{H}}^T \tilde{\Sigma}^{-1} \mathbf{vec}(\mathbf{Y}) \\
&= \mathbf{H} \mathbf{Diag}(\mathbf{k}_i^T) \left[ \mathbf{Diag}(\mathbf{K}_i) + \Sigma_P \otimes \mathbf{I}_n \right]^{-1} \mathbf{vec}(\mathbf{Y} \Sigma^{-1} \mathbf{H} \Sigma_P^{-1})
\end{aligned}$$

The first equality is from the above considerations ; the second is from Woodburry's identity ; the sixth is a backward application of Woodburry's identity ; and the last is an application of fact (12).

We now turn to the expected variance, setting further notations  $\mathbb{K} = \mathbf{Diag}(\mathbf{K}_i)$  and  $\mathfrak{K} = \mathbf{Diag}(\mathbf{k}_i)$  for compacity:

$$\begin{aligned}
\mathbf{k}_{**} - \mathbf{k}_*^T \mathcal{K}^{-1} \mathbf{k}_* &= \mathbf{H} \mathbf{Diag}(\mathbf{k}_{i**}) \mathbf{H}^T - \mathbf{H} \mathfrak{K}^T \tilde{\mathbf{H}}^T \left( \tilde{\mathbf{H}} \mathbb{K} \tilde{\mathbf{H}}^T + \tilde{\Sigma} \right)^{-1} \tilde{\mathbf{H}} \mathfrak{K} \mathbf{H}^T \\
&= \mathbf{H} \left[ \mathbf{Diag}(\mathbf{k}_{i**}) - \mathfrak{K}^T \tilde{\mathbf{H}}^T \left( \tilde{\mathbf{H}} \mathbb{K} \tilde{\mathbf{H}}^T + \tilde{\Sigma} \right)^{-1} \tilde{\mathbf{H}} \mathfrak{K} \right] \mathbf{H}^T \\
&= \mathbf{H} \left[ \mathbf{Diag}(\mathbf{k}_{i**}) - \mathfrak{K}^T \left( \mathbb{K} + \tilde{\Sigma}_P \right)^{-1} \mathfrak{K} \right] \mathbf{H}^T \\
&= \mathbf{H} \left[ \mathbf{Diag}(\mathbf{k}_{i**}) - \mathbf{Diag}(\mathbf{k}_{i*}^T) \left[ \mathbf{Diag}(\mathbf{K}_i) + (\mathbf{H}^T \Sigma^{-1} \mathbf{H})^{-1} \otimes \mathbf{I}_n \right]^{-1} \mathbf{Diag}(\mathbf{k}_{i*}) \right] \mathbf{H}^T
\end{aligned}$$

The first equality is from the above considerations, and the third is lemma 3. □

## F.4 Alternate expression of the likelihood

We here propose an expression for the marginal log-likelihood inspired by Gu and Shen [2020]. It's less convenient than this of prop.9 as it doesn't boil down to MLLs of single-output GPs, but it shows that

<sup>13</sup>This can be seen by writing explicitly the coordinates of  $\mathbf{K} = \sum_{i=1}^q \mathbf{B}_i \otimes \mathbf{K}_i$ , reminding that  $\mathbf{B}_i = \mathbf{H}_i \mathbf{H}_i^T$  (where  $\mathbf{H}_i$  is the  $i$ -th column of  $\mathbf{H}$ ).

a latent-revealing expression which decouples under the DPN hypothesis can be obtained from elementary manipulations.

**Proposition 12.** *In all generality of the LMC model, it stands:*

$$\begin{aligned} -2 \log p(\mathbf{Y}) &= \sum_{j=1}^n \mathbf{Y}_j \boldsymbol{\Sigma}^{-1} \mathbf{Y}_j^{\mathbf{T}} - \text{vec}(\mathbf{Y}^{\mathbf{T}} \boldsymbol{\Sigma}^{-1} \mathbf{H})^{\mathbf{T}} (\text{Diag}(\mathbf{K}_i^{-1}) + \boldsymbol{\Sigma}_{\mathbf{P}}^{-1} \otimes \mathbf{I}_n)^{-1} \text{vec}(\mathbf{Y}^{\mathbf{T}} \boldsymbol{\Sigma}^{-1} \mathbf{H}) \\ &\quad + \log |\text{Diag}(\mathbf{K}_i) + \boldsymbol{\Sigma}_{\mathbf{P}} \otimes \mathbf{I}_n| + 2n \log |\mathbf{R}| + n \log |\tilde{\mathbf{B}}| + np \log 2\pi \end{aligned}$$

The DPN condition is necessary and sufficient for this expression to decouple between latent processes: it then holds  $|\text{Diag}(\mathbf{K}_i) + \boldsymbol{\Sigma}_{\mathbf{P}} \otimes \mathbf{I}_n| = \prod_{i=1}^q |\mathbf{K}_i + \sigma_i \mathbf{I}_n|$ , and

$$\text{vec}(\mathbf{Y}^{\mathbf{T}} \boldsymbol{\Sigma}^{-1} \mathbf{H})^{\mathbf{T}} (\text{Diag}(\mathbf{K}_i^{-1}) + \boldsymbol{\Sigma}_{\mathbf{P}}^{-1} \otimes \mathbf{I}_n)^{-1} \text{vec}(\mathbf{Y}^{\mathbf{T}} \boldsymbol{\Sigma}^{-1} \mathbf{H}) = \sum_{i=1}^q \mathbf{H}_i \boldsymbol{\Sigma}^{-1} \mathbf{Y} (\mathbf{K}_i^{-1} + \sigma_i^{-1} \mathbf{I}_n)^{-1} \mathbf{Y}^{\mathbf{T}} \boldsymbol{\Sigma}^{-1} \mathbf{H}_i^{\mathbf{T}}.$$

*Proof.* We start by expressing the MLL in the most straightforward way :

$$-2 \log p(\mathbf{Y}) = \mathbf{Y}_{\mathbf{v}}^{\mathbf{T}} \mathcal{K}^{-1} \mathbf{Y}_{\mathbf{v}} + \log |\mathcal{K}| + \frac{np}{2} \log \pi ,$$

with  $\mathcal{K} = (\mathbf{H} \otimes \mathbf{I}_n) \text{Diag}(\mathbf{K}_i) (\mathbf{H}^{\mathbf{T}} \otimes \mathbf{I}_n) + \boldsymbol{\Sigma} \otimes \mathbf{I}_n$  as before. We deal with the first term by applying Woddburry's formula :

$$\begin{aligned} \mathbf{Y}_{\mathbf{v}}^{\mathbf{T}} \mathcal{K}^{-1} \mathbf{Y}_{\mathbf{v}} &= \mathbf{Y}_{\mathbf{v}}^{\mathbf{T}} (\boldsymbol{\Sigma}^{-1} \otimes \mathbf{I}_n) \mathbf{Y}_{\mathbf{v}} - \mathbf{Y}_{\mathbf{v}}^{\mathbf{T}} (\boldsymbol{\Sigma}^{-1} \mathbf{H} \otimes \mathbf{I}_n) (\text{Diag}(\mathbf{K}_i^{-1}) + \boldsymbol{\Sigma}_{\mathbf{P}}^{-1} \otimes \mathbf{I}_n)^{-1} (\mathbf{H}^{\mathbf{T}} \boldsymbol{\Sigma}^{-1} \otimes \mathbf{I}_n) \mathbf{Y}_{\mathbf{v}} \\ &= \sum_{j=1}^n \mathbf{Y}_j \boldsymbol{\Sigma}^{-1} \mathbf{Y}_j^{\mathbf{T}} - \text{vec}(\mathbf{Y}^{\mathbf{T}} \boldsymbol{\Sigma}^{-1} \mathbf{H})^{\mathbf{T}} (\text{Diag}(\mathbf{K}_i^{-1}) + \boldsymbol{\Sigma}_{\mathbf{P}}^{-1} \otimes \mathbf{I}_n)^{-1} \text{vec}(\mathbf{Y}^{\mathbf{T}} \boldsymbol{\Sigma}^{-1} \mathbf{H}) \end{aligned}$$

For the log-determinant, we use the parametrization of section 4:

$$\begin{aligned} |\mathcal{K}| &= |\mathbf{Q}_+ \mathbf{R}_+ \otimes \mathbf{I}_n| |\mathbf{D}_+ \otimes \mathbf{I}_n + \text{Diag}(\mathbf{K}_i)| |\mathbf{R}_+^{\mathbf{T}} \mathbf{Q}_+^{\mathbf{T}} \otimes \mathbf{I}_n| \\ &= |\mathbf{R}_+|^n |\mathbf{D}_+ \otimes \mathbf{I}_n + \text{Diag}(\mathbf{K}_i)| |\mathbf{R}_+|^n \quad \text{because } |\mathbf{Q}_+| = 1 \text{ and by the properties of the Kronecker product} \\ &= |\mathbf{R}|^{2n} |\tilde{\mathbf{B}} \otimes \mathbf{I}_n| \left| (\text{Diag}(\mathbf{K}_i) + \tilde{\mathbf{D}} \otimes \mathbf{I}_n) - \tilde{\mathbf{M}} \tilde{\mathbf{B}}^{-1} \tilde{\mathbf{M}}^{\mathbf{T}} \otimes \mathbf{I}_n \right| \quad \text{by Schur's determinant formula} \\ &= |\mathbf{R}|^{2n} |\tilde{\mathbf{B}}|^n |\text{Diag}(\mathbf{K}_i) + (\tilde{\mathbf{D}} - \tilde{\mathbf{M}} \tilde{\mathbf{B}}^{-1} \tilde{\mathbf{M}}^{\mathbf{T}}) \otimes \mathbf{I}_n| \\ &= |\mathbf{R}|^{2n} |\tilde{\mathbf{B}}|^n |\text{Diag}(\mathbf{K}_i) + \boldsymbol{\Sigma}_{\mathbf{P}} \otimes \mathbf{I}_n| \quad \text{by block-matrix formulas} \end{aligned}$$

which yields the desired result. For the second equality, note that the block decomposition of  $\mathbf{D}_+ \otimes \mathbf{I}_n + \text{Diag}(\mathbf{K}_i)$  (in blocks of size  $nq \times nq$ ,  $nq \times n(p-q)$ , etc) is  $\left( \begin{array}{c|c} \text{Diag}(\mathbf{K}_i) + \tilde{\mathbf{D}} \otimes \mathbf{I}_n & \tilde{\mathbf{M}} \otimes \mathbf{I}_n \\ \hline \tilde{\mathbf{M}}^{\mathbf{T}} \otimes \mathbf{I}_n & \tilde{\mathbf{B}} \otimes \mathbf{I}_n \end{array} \right)$ .  $\square$

## G Restrictivity of the DPN hypothesis

This short paragraph aims at assessing the severity of the DPN hypothesis. It consists mainly of the following proposition :

**Proposition 13.** Let  $\Sigma_{\text{opt}}$  the value of  $\Sigma$  which optimizes the MLL of the unconstrained LMC model. Let  $\Sigma_{\text{opt}}^{-1} = \mathbf{Q}\mathbf{A}\mathbf{Q}^T + \mathbf{Q}_{\perp}\mathbf{B}\mathbf{Q}_{\perp}^T + 2\text{Sym}(\mathbf{Q}\mathbf{C}\mathbf{Q}_{\perp}^T)$  be the decomposition of  $\Sigma_{\text{opt}}^{-1}$  as in prop.1. Then the minimal distance between  $\Sigma_{\text{opt}}^{-1}$  and a precision matrix  $\Sigma_{\text{app}}$  compatible with the DPN hypothesis is :

$$\min_{\Sigma_{\text{app}}} \|\Sigma_{\text{opt}}^{-1} - \Sigma_{\text{app}}^{-1}\|_F^2 = \min_{\mathbf{D}} \|\mathbf{A} - \mathbf{R}^{-T}\mathbf{D}\mathbf{R}^{-1}\|_F^2 \quad \text{subject to } \mathbf{D} \text{ positive and diagonal,} \quad (19)$$

where  $\|\cdot\|_F$  denotes the Frobenius norm. It is minimized for  $\Sigma_{\text{app}}^{-1} = \mathbf{Q}\mathbf{R}^{-T}\mathbf{D}'\mathbf{R}^{-1}\mathbf{Q}^T + \mathbf{Q}_{\perp}\mathbf{B}\mathbf{Q}_{\perp}^T + 2\text{Sym}(\mathbf{Q}\mathbf{C}\mathbf{Q}_{\perp}^T)$ , where  $\mathbf{D}' = \text{Diag}[(\mathbf{R}^{-1}\mathbf{R}^{-T} \odot \mathbf{R}^{-1}\mathbf{R}^{-T})^{-1}\text{diag}(\mathbf{R}^{-1}\mathbf{A}\mathbf{R}^{-T})]$  is the optimal  $\mathbf{D}$  in the above expression,  $\text{diag}$  is the operator taking the diagonal of a square matrix (into vector form) and  $\odot$  denotes the Hadamard product (elementwise matrix product).

*Proof.* Let's write  $\Sigma_{\text{app}}^{-1} = \mathbf{Q}\mathbf{A}'\mathbf{Q}^T + \mathbf{Q}_{\perp}\mathbf{B}'\mathbf{Q}_{\perp}^T + 2\text{Sym}(\mathbf{Q}\mathbf{C}'\mathbf{Q}_{\perp}^T)$  the decomposition of  $\Sigma_{\text{app}}^{-1}$ . It is a general property that the Frobenius norm of a symmetric matrix can be computed blockwise, that is :

$$\min_{\Sigma_{\text{app}}} \|\Sigma_{\text{opt}}^{-1} - \Sigma_{\text{app}}^{-1}\|_F^2 = \text{Tr}((\Sigma_{\text{opt}}^{-1} - \Sigma_{\text{app}}^{-1})^2) = \text{Tr}((\mathbf{A} - \mathbf{A}')^2) + \text{Tr}((\mathbf{B} - \mathbf{B}')^2) + 2\text{Tr}((\mathbf{C} - \mathbf{C}')(\mathbf{C} - \mathbf{C}')^T)$$

This can be shown either by writing the norm as a sum of squared coefficients and splitting the sum at the right indices, or by replacing  $\Sigma_{\text{opt}}^{-1}$  and  $\Sigma_{\text{app}}^{-1}$  by their decompositions, expanding the trace of their squared difference and eliminating all cross-coefficients because of the circularity of the trace (i.e :  $\text{Tr}(\mathbf{X}\mathbf{Q}\mathbf{Q}_{\perp}^T) = \text{Tr}(\mathbf{X}\mathbf{Q}_{\perp}^T\mathbf{Q}) = 0$ ). Also recall that the trace is conjugation-invariant :  $\text{Tr}(\mathbf{Q}(\mathbf{A} - \mathbf{A}')^2\mathbf{Q}^T) = \text{Tr}((\mathbf{A} - \mathbf{A}')^2)$ , etc.

Prop. 6 showed that the DPN hypothesis doesn't put any constraints on  $\mathbf{B}$  and  $\mathbf{C}$ . Therefore, one can simply set  $\mathbf{B}' = \mathbf{B}$  and  $\mathbf{C}' = \mathbf{C}$  to zero their contribution to the discrepancy. Proposition 6 also shows that the DPN hypothesis is equivalent to  $(\mathbf{A}' = \mathbf{R}^{-T}\mathbf{D}\mathbf{R}^{-1}$  for some diagonal matrix  $\mathbf{D}$ ), hence equation (19).

In order to find the optimal  $\mathbf{D}$ , we set additional notations :  $\mathbf{D} = \text{Diag}(\mathbf{v})$  ;  $\|\mathbf{A} - \mathbf{R}^{-T}\mathbf{D}\mathbf{R}^{-1}\|_F^2 = \|\Delta\|_F^2 = \Phi(\Delta)$ ;  $\mathbf{M} : \mathbf{N} = \text{Tr}(\mathbf{M}^T\mathbf{N})$  denotes the Frobenius scalar product. We then compute the differential, considering  $\mathbf{v}$  as the only variable:

$$\begin{aligned} d\Phi &= 2\Delta : d\Delta = 2\Delta : d(\mathbf{R}^{-T}\text{Diag}(\mathbf{v})\mathbf{R}^{-1}) = 2\Delta : \mathbf{R}^{-T}d(\text{Diag}(\mathbf{v}))\mathbf{R}^{-1} \\ &= 2\mathbf{R}^{-1}\Delta\mathbf{R}^{-T} : d(\text{Diag}(\mathbf{v})) = 2\mathbf{R}^{-1}\Delta\mathbf{R}^{-T} : \text{Diag}(d\mathbf{v}) = 2\text{diag}(\mathbf{R}^{-1}\Delta\mathbf{R}^{-T}) : d\mathbf{v} \end{aligned}$$

All of these expressions are standard manipulations involving differentials and scalar products; see for instance Petersen and Pedersen [2012]. The last one,  $\mathbf{X} : \text{Diag}(\mathbf{y}) = \text{diag}(\mathbf{X}) : \mathbf{y}$ <sup>14</sup> is less standard : it can be proved by direct expansion in matrix coefficients.

The last expression defines the gradient of  $\Phi$  with respect to the vector  $\mathbf{v}$  :  $d\Phi = 2\text{diag}(\mathbf{R}^{-1}\Delta\mathbf{R}^{-T}) : d\mathbf{v} \Leftrightarrow \nabla_{\mathbf{v}}\Phi = \text{diag}(\mathbf{R}^{-1}\Delta\mathbf{R}^{-T})$ . We can then set this gradient to zero to find the global minimum :

$$\begin{aligned} \nabla_{\mathbf{v}}\Phi = 0 &\Leftrightarrow \text{diag}(\mathbf{R}^{-1}\Delta\mathbf{R}^{-T}) = 0 \Leftrightarrow \text{diag}(\mathbf{R}^{-1}\mathbf{A}\mathbf{R}^{-T}) = \text{diag}(\mathbf{R}^{-1}\mathbf{R}^{-T}\text{Diag}(\mathbf{v})\mathbf{R}^{-1}\mathbf{R}^{-T}) \\ &\Leftrightarrow \text{diag}(\mathbf{R}^{-1}\mathbf{A}\mathbf{R}^{-T}) = ((\mathbf{R}^{-1}\mathbf{R}^{-T}) \odot (\mathbf{R}^{-1}\mathbf{R}^{-T})) \mathbf{v} \\ &\Leftrightarrow \mathbf{v} = (\mathbf{R}^{-1}\mathbf{R}^{-T} \odot \mathbf{R}^{-1}\mathbf{R}^{-T})^{-1}\text{diag}(\mathbf{R}^{-1}\mathbf{A}\mathbf{R}^{-T}) \end{aligned}$$

<sup>14</sup>Where we recall that  $\text{diag}(\mathbf{X})$  denotes the diagonal of matrix  $\mathbf{X}$  while  $\text{Diag}(\mathbf{y})$  is the diagonal square matrix made from the vector  $\mathbf{y}$ .

The second-to-last equivalence is from another unusual matrix identity :  $\mathbf{diag}(\mathbf{X} \mathbf{Diag}(\mathbf{v}) \mathbf{Y}) = (\mathbf{Y}^T \odot \mathbf{X}) \mathbf{v}$ . Here again, the proof is by direct expansion of the matrix coefficients.  $\square$

Proposition 13 proves what was previously stated in a more informal way : the discrepancy between the DPN-restricted model and the unrestricted one lies only in an approximation of the "true" matrix  $\mathbf{A}$ . The fact that the minimizer of this discrepancy has a simple form paves the way for an eventual *correction procedure* for the noise : if the data is assumed to exhibit a specific noise structure which is not diagonally projectable, one could parametrize such an optimal noise  $\Sigma_{\text{opt}}$  in addition to the noise parameters  $\tilde{\mathbf{B}}$ ,  $\mathbf{M}$  and  $\Sigma_{\mathbf{P}}$ . One would then add to the likelihood a term proportional to  $n \times \mathbf{diag}(\mathbf{Q}^T \Sigma_{\text{opt}}^{-1} \mathbf{Q} - \mathbf{R}^{-T} \Sigma_{\mathbf{P}}^{-1} \mathbf{R}^{-1})$  (reminding that  $\mathbf{D} = \Sigma_{\mathbf{P}}^{-1}$  and  $\mathbf{A} = \mathbf{Q}^T \Sigma^{-1} \mathbf{Q}$ ), which would warp the model towards a more realistic noise. Alternately, an interleaved optimization scheme could be developed, in the spirit of a projected gradient descent: at each iteration, one would estimate a DPN-compatible noise  $\Sigma_{\text{app}}$  by optimizing the MLL of prop.10, find the nearest noise  $\Sigma_{\text{opt}}$  (or at least a near one) enforcing the desired noise structure, compute its decomposition in terms of  $\mathbf{A}$ ,  $\mathbf{B}$  and  $\mathbf{C}$ , and then come back to the initial variables by setting  $\mathbf{B} \leftarrow \mathbf{B}$ ,  $\mathbf{C} \leftarrow \mathbf{C}$  and  $\Sigma_{\mathbf{P}}^{-1} = \mathbf{Diag}(\mathbf{v}) \leftarrow \mathbf{Diag}[(\mathbf{R}^{-1} \mathbf{R}^{-T} \odot \mathbf{R}^{-1} \mathbf{R}^{-T})^{-1} \mathbf{diag}(\mathbf{R}^{-1} \mathbf{A} \mathbf{R}^{-T})]$ . This is beyond the scope of this article and has not been experimented on yet, by lack of a relevant study case.

## H Interpretation : comparison with other LMC approximations

### H.1 Relation to variational approaches

We wish to underline a link between previous results and the apparently unrelated variational methods for GPs. The latter are widespread tools to handle multitask GPs, yet the exact nature and cause of the computational gains they offer is not always clear. The focus is often on the reduction of kernel size thanks to the inducing points paradigm, and on the fact that the ELBO (approximate likelihood) factorizes over datapoints. But there is another major source of gains: *variational multi-output GPs implicitly decouple latent processes*. Although a formal exposition of the variational GP framework is beyond the scope of this paper, we can show this in a few expressions using standard notations. If  $\mathbf{f}_i$  represents the values of latent process  $i$  at observation points,  $\mathbf{u}_i$  its values at pseudo-input points, variational models introduce approximate posteriors  $q(\mathbf{u}_i) = \mathcal{N}(\mathbf{u}_i | \mathbf{m}_i, \mathbf{S}_i)$  ( $\mathbf{m}_i, \mathbf{S}_i$  being parameters of the model) such that  $q(\mathbf{u}_i) \simeq p(\mathbf{u}_i, \mathbf{f}_i | \mathbf{y})$ .

The key point here is that it is always assumed (but not always emphasized) that the global approximate posterior  $q(\mathbf{u})$  factorizes over latent processes:  $q(\mathbf{u}) = \prod_{i=1}^q q(\mathbf{u}_i)$ . This construction makes all posteriors and likelihood terms factorize too: what in the original LMC is a condition (which we have shown to be equivalent to the DPN condition) is automatically enforced in its variational counterpart.

We also wish to underline the analogy between our posterior estimators and these of the variational model, which can be found for instance in Liu et al. [2023] or Liu et al. [2022];  $p(\mathbf{u}_i, \mathbf{f}_i | \mathbf{y}) \simeq q(\mathbf{f}_i) = \mathcal{N}(\mu_i, \nu_i)$ , with :

$$\mu_i = \mathbf{k}_{i*}^T \mathbf{K}_i^{-1} \mathbf{m}_i \quad (20)$$

$$\nu_i = k_{i**} - \mathbf{k}_{i*}^T (\mathbf{K}_i^{-1} - \mathbf{K}_i^{-1} \mathbf{S}_i \mathbf{K}_i^{-1}) \mathbf{k}_{i*} = k_{i**} - \mathbf{k}_{i*}^T \left( \mathbf{K}_i^{-1} - \mathbf{K}_i^{-1} (\mathbf{K}_i^{-1} + (\mathbf{S}_i^{-1} - \mathbf{K}_i^{-1}))^{-1} \mathbf{K}_i^{-1} \right) \mathbf{k}_{i*} \quad (21)$$

$$= k_{i**} - \mathbf{k}_{i*}^T (\mathbf{K}_i + (\mathbf{S}_i^{-1} - \mathbf{K}_i^{-1})^{-1})^{-1} \mathbf{k}_{i*} \text{ by the previously-used Woodburry-type equality,} \quad (22)$$

where the covariance vector and matrix are here evaluated at pseudo-input points rather than observed datapoints. We notice the direct similarity with the decoupled expressions of prop.4, simply replacing  $\mathbf{Y}\mathbf{T}_i$  by  $\mathbf{m}_i$  and  $\sigma_i^2 \mathbf{I}_n$  by  $(\mathbf{S}_i^{-1} - \mathbf{K}_i^{-1})^{-1}$  (and the real observation points by their pseudo-input counterparts): **the variational model learns additional parameters** (these of the approximate posterior,  $\mathbf{m}_i$  and  $\mathbf{S}_i$ ) **which substitute themselves to the projected data and projected noise.**

## H.2 Relation to the ICM model

In this paragraph, we answer the following interrogation : are computational gains of the ICM (relative to the naive LMC implementation) due to some sort of decoupling of the latent processes ? This question seems natural, as the ICM simplifies the latent process structure compared to the LMC. However, the answer is negative : the simplification is this time of another kind.

The ICM is defined by its covariance matrix  $\mathbf{K} = \mathbf{K}_T \otimes \mathbf{K}_x$ , as opposed to this of the LMC as defined above in the matricial proof F.3 of prop.2:  $\mathbf{K} = \sum_{i=1}^q \mathbf{B}_i \otimes \mathbf{K}_i$ . This corresponds to all latent processes sharing the same kernel : if  $\mathbf{K}_i = \mathbf{K}_x \forall i$  in the latter expression, we recover the ICM by setting  $\mathbf{K}_T = \sum_{i=1}^q \mathbf{B}_i$ . As  $\mathbf{K}^{-1} = \mathbf{K}_T^{-1} \otimes \mathbf{K}_x^{-1}$  one could think that this covariance structure trivializes all computations, but this is not the case because of the noise: the noise-added covariance  $\mathcal{K} = \mathbf{K}_T \otimes \mathbf{K}_x + \Sigma \otimes \mathbf{I}_n$  is still not easily invertible. Additional tricks are thus necessary to carry efficient computation ; we comment here on the approach of Rakitsch et al. [2013], as it is exact and more efficient than the original model of Bonilla et al. [2007], which only uses low-rank approximations of  $\mathbf{K}_T$  and  $\mathbf{K}_x$ .

If we frame the ICM as a particular case of LMC like we did above, we get that  $\mathbf{K}_T = \mathbf{H}\mathbf{H}^T$  (because  $\mathbf{B}_i = \mathbf{H}_i \mathbf{H}_i^T$ ). We define  $\mathbf{U}_H \mathbf{S}_H^2 \mathbf{U}_H^T$  as the diagonalization of  $\mathbf{K}_T$ <sup>15</sup>, and  $\Sigma = \mathbf{U}_\Sigma \mathbf{S}_\Sigma \mathbf{U}_\Sigma^T$  the diagonalization of  $\Sigma$ <sup>16</sup>. We can then compare our approach with this of Rakitsch et al. [2013], which is all contained in the following decomposition (equation (7) of said paper<sup>17</sup>):

$$\mathcal{K} = \mathbf{K}_T \otimes \mathbf{K}_x + \Sigma \otimes \mathbf{I}_n = \left( \mathbf{U}_\Sigma \mathbf{S}_\Sigma^{\frac{1}{2}} \otimes \mathbf{I}_n \right) \left( \mathbf{S}_\Sigma^{-\frac{1}{2}} \mathbf{U}_\Sigma^T \mathbf{K}_T \mathbf{U}_\Sigma \mathbf{S}_\Sigma^{-\frac{1}{2}} \otimes \mathbf{K}_x + \mathbf{I}_p \otimes \mathbf{I}_n \right) \left( \mathbf{S}_\Sigma^{\frac{1}{2}} \mathbf{U}_\Sigma^T \otimes \mathbf{I}_n \right) \quad (23)$$

The purpose of this factorization is to exploit the convenient properties of  $\mathbf{I}_p \otimes \mathbf{I}_n$  : for any symmetric matrices  $\mathbf{S}, \mathbf{S}'$  of eigen-decompositions  $\mathbf{U}\mathbf{D}\mathbf{U}^T$  and  $\mathbf{U}'\mathbf{D}'\mathbf{U}'^T$ , we get that the eigen-decomposition of  $(\mathbf{S} \otimes \mathbf{S}' + \mathbf{I} \otimes \mathbf{I})$  is  $(\mathbf{U} \otimes \mathbf{U}') \left( \mathbf{D} \otimes \mathbf{D}' + \mathbf{I} \otimes \mathbf{I} \right) (\mathbf{U}^T \otimes \mathbf{U}'^T)$ . The fact that the eigenvectors of the large

<sup>15</sup>Careful inspection shows that in the ICM, if  $\mathbf{U}_H \mathbf{S}_H \mathbf{V}_H^T$  is the singular values decomposition of  $\mathbf{H}$ , it can be assumed in all generality that  $\mathbf{V}_H = \mathbf{I}_n$ , all latent processes sharing the same kernel; this is used in equation 26.

<sup>16</sup>In these definitions  $\mathbf{S}_H$  is squared for coherency with the rest of the present paper, while  $\mathbf{S}_\Sigma$  is not to keep the notations of Rakitsch et al. [2013].

<sup>17</sup>Where we have made the restriction  $\Omega = \mathbf{I}_n$  for reading purposes, corresponding to homoskedastic noise.

matrix are Kronecker products authorizes easy manipulation and fast computation; this is the approach followed by Rakitsch to perform all calculations.

On the other side, our approach relies on a different implicit factorization. For the sake of comparison, we apply it to the ICM covariance structure, which yields :

$$\mathcal{K} = \mathbf{H}\mathbf{H}^T \otimes \mathbf{K}_x + \Sigma \otimes \mathbf{I}_n \simeq (\mathbf{U}_H \mathbf{S}_H \otimes \mathbf{I}_n) (\mathbf{I}_q \otimes \mathbf{K}_x + \mathbf{S}_H^{-1} \mathbf{U}_H^T \Sigma \mathbf{U}_H \mathbf{S}_H^{-1} \otimes \mathbf{I}_n) (\mathbf{S}_H \mathbf{U}_H^T \otimes \mathbf{I}_n) \quad (24)$$

$$= (\mathbf{H} \otimes \mathbf{I}_n) (\mathbf{I}_q \otimes \mathbf{K}_x + \mathbf{H}^+ \Sigma \mathbf{H}^{+T} \otimes \mathbf{I}_n) (\mathbf{H}^T \otimes \mathbf{I}_n) \quad (25)$$

$$\simeq (\mathbf{H} \otimes \mathbf{I}_n) (\mathbf{Diag}(\mathbf{K}_x) + \Sigma_P \otimes \mathbf{I}_n) (\mathbf{H}^T \otimes \mathbf{I}_n) \quad (26)$$

where  $\mathbf{H}^+$  denotes the Moore-Penrose pseudoinverse of  $\mathbf{H}$ . This factorization is not rigorous as it is rank-deficient; it nonetheless appears in the matricial proof F.3 of prop.2, where is it made rigorous by two successive applications of Woodburry-like formulas involving other terms<sup>18</sup> Besides this occurrence, factorization (26) illustrates the core of our approach : the noise-augmented covariance can be summarized by a latent block-diagonal term of size  $qn \times qn$ , left- and right-multiplied by the mixing matrix.

Comparing the above equations shows both the analogy and difference between the two approaches. Ours relies on left- and right-factorization of the the eigen-decomposition of the *task* covariance matrix; the term  $\mathbf{H}^+ \Sigma \mathbf{H}^{+T}$  – in reality  $\mathbf{T} \Sigma \mathbf{T}^T$  with a more rigorous derivation – has to be diagonal for the central term to be computationally efficient, hence the DPN hypothesis. On the other hand, the approach of Rakitsch factorizes the eigen-decomposition of the *noise* covariance matrix; then the central term is always easy to handle because of the  $\mathbf{I}_p \otimes \mathbf{I}_n$  term, and no additional hypothesis is necessary to attain a  $O(n^3 + p^3)$  complexity. Note however that *factorization (23) requires the GP covariance matrix to be a Kronecker product* : it is thus restricted to the ICM model.

We finally emphasize that latent processes are *not* independant conditionally on observations in the ICM: we have already shown this property to be equivalent to the DPN condition, and the present section illustrates that the DPN condition is not automatically enforced by the ICM,  $\mathbf{H}$  and  $\Sigma$  still being arbitrary in this model.

---

<sup>18</sup>More exactly, in said derivation  $\mathbf{I}_q \otimes \mathbf{K}_x$  is replaced by  $\mathbf{Diag}(\mathbf{K}_i)$  (because there latent processes have different kernels), and  $\mathbf{H}^+$  is replaced by  $\mathbf{T}$ , which we recall to be another generalized inverse of  $\mathbf{H}$  (it even stands  $\mathbf{T} = \mathbf{H}^+$  under the BDN assumption 2).